Report no. changed (Mar 2006): SR-299-UU

SACLANTCEN REPORT
serial no: SR-299

SACLANT UNDERSEA
RESEARCH CENTRE
REPORT

OCEANOGRAPHIC CONDITIONS IN THE ANTALYA BASIN IN WATER

R. Onken

July 1998

SACLANT Undersea Research Centre
Viale San Bartolomeo 400
19138 San Bartolomeo (SP), Italy

tel: +39-0187-540.111
fax: +39-0187-524.600

e-mail: library@saclantc.nato.int

NORTH ATLANTIC TREATY ORGANIZATION

Report no. changed (Mar 2006): SR-299-UU

Oceanographic conditions in the Antalya Basin in winter

Reiner Onken

The content of this document pertains to work performed under Project 022-3 of the SACLANTCEN Programme of Work. The document has been approved for release by The Director, SACLANTCEN.

Jan L. Spoelstra
Director

intentionally blank page

Oceanographic conditions in the Antalya Basin in winter

Reiner Onken

Executive Summary: In February 1997 a high resolution survey of the northeastern Levantine Sea was conducted by *NRV Alliance* and the Turkish vessel *TCG Çubuklu*. The objective of the trial was to improve the knowledge and understanding of the oceanic environment within the northeastern Levantine Sea in late winter.

The Asia Minor Current (AMC), the Cilician Current (CC), and two anticyclonic eddies in the central Antalya Basin and between the Anaximander Seamounts and the Turkish coast were the dominant features of the large-scale current system. While the position of the anticyclones was rather stationary, rapidly travelling meanders were characteristic features of the AMC and the CC. Both currents were identified by a well defined front (AMC front) in the temperature and salinity field. In the central parts of the anticyclones, large homogeneous pools of warm and saline water were found between the sea surface and about 250 m depth, whereas the region occupied by the AMC and CC was more stratified.

The sound velocity profile, which controls underwater detection conditions, exhibits spatial and temporal changes in tactically relevant scales. The AMC front separated two completely different regimes of sound velocity. South of the front the sound velocity decreases continuously from the sea surface down to the axis of the main sound channel located at about 300 m depth. In contrast, north of the front the sound velocity is characterized by an intermediate maximum between 200 and 300 m depth. Within the frontal region, the sound velocity structure changes rapidly due to the meander activity.

intentionally blank page

Oceanographic conditions in the Antalya Basin in winter

Reiner Onken

Abstract: From an oceanographic survey of the Anatalya Basin in February 1997 the following horizontal circulation pattern was found: The Asia Minor Current (AMC) was detached from the Turkish coast flowing to the southwest between 30°E and 33°E. The Cilician Current was present and feeding the AMC. The AMC exhibited meander wavelengths of about 100 km and phase speed circa 10 cm s^{-1}. A train of cyclonic eddies was located at the southern flank of the AMC. The central part of the Antalya Basin was occupied by the Antalya Anticyclone extending at least over the upper 1000 dbar depth range. A second anticyclone further west was identified as the Anaximander Anticyclone. From a comparison with previous surveys it is concluded that the circulation of the Antalya Basin is controlled by the position of the AMC. The circulation is cyclonic, if the AMC flow path is confined to the coast, and anticyclonic, if the path is distant from coast. In the latter case, the anticyclonic flow may force the Cilician Current to reverse its direction.

A nearly homogeneous pool of Levantine Surface Water extending down from the sea surface to about 250 m depth was found trapped within the Antalya Anticyclone. It is shown that even under light wind conditions, thermohaline convection down to about 200 m depth takes place in this pool. It is suggested that the convectively mixed water body is subject to further transformation by double diffusive mixing with the underlying water and finally contributes to the formation of Levantine Intermediate Water.

Keywords: eastern Mediterranean ○ Levantine Basin ○ Antalya Basin ○ Antalya Anticyclone ○ Anaximander Anticyclone ○ Asia Minor Current ○ Cilician Current ○ Levantine Intermediate Water ○ circulation ○ convection ○ sound velocity ○ variability

Contents

List of Figures

List of Tables

1

Introduction

The Antalya Basin lies in the northern Levantine Basin (Figure 1), which with the Ionian Basin and the Adriatic and Aegean Seas forms the eastern Mediterranean Sea. This study is based on a hydrographic survey conducted in February 1997 by the NATO SACLANT Undersea Research Centre in collaboration with the Turkish Navy Department of Navigation, Hydrography and Oceanography (Istanbul).

Until the late 1980s, knowledge of the large scale circulation of the upper layers of the eastern Mediterranean was limited. Considerable progress was achieved by the POEM (Physical Oceanography of the eastern Mediterranean) experiment ([2], [3], [1]). From these surveys, it emerged that Modified Atlantic Water (AW) enters the Ionian Basin through the Strait of Sicily as Atlantic–Ionian Stream (AIS), meanders through the Ionian Basin and then traverses the Levantine Basin as Mid-Mediterranean Jet (MMJ) (Figure 2). The MMJ is accompanied by sub-basin-scale anticyclonic recirculation eddies to the south and cyclonic eddies to the north of the jet axis. The major northern cyclones are the Rhodes Cyclone, southeast of Rhodes and the West Cyprus Cyclone, occupying a large part of the Antalya Basin, both cyclones are assumed to be permanent features of the general circulation. At the northern flank, close to the Turkish coast, the latter cyclones are interconnected by the westward flowing Asia Minor Current (AMC), which is fed by the Cilician Current (CC) heading westward between Cyprus and Turkey. In contrast to the AMC, the CC is classified as a recurrent or transient feature, because it was not verified in all surveys conducted during the 1985–1988 period. Similarly, anticyclonic eddies appear to be transient features of the Antalya Basin circulation. [2] found a strong, depth intensified, anticyclonic eddy dominating the Antalya Basin circulation in October/November 1985. Another anticyclone was found in the 1985 data between the Anaximander Seamounts (Figure 1) and the Turkish coast (to be referred to as Anaximander Anticyclone (AxAC)). Anticyclonic eddies, less intense and in position slightly different, were also identified in the March/April and June 1986 data, which also verify that the West Cyprus Cyclone does not extend beyond about 35°N. [4] also show a strong anticyclone covering the western part of the Antalya Basin in June 1987, which feature was not present in late summer of the same year, when the entire Antalya Basin exhibits a cyclonic circulation.

The surface waters of the eastern Mediterranean are subject to strong transformation processes due to the interaction with the atmosphere. In summer, there is a

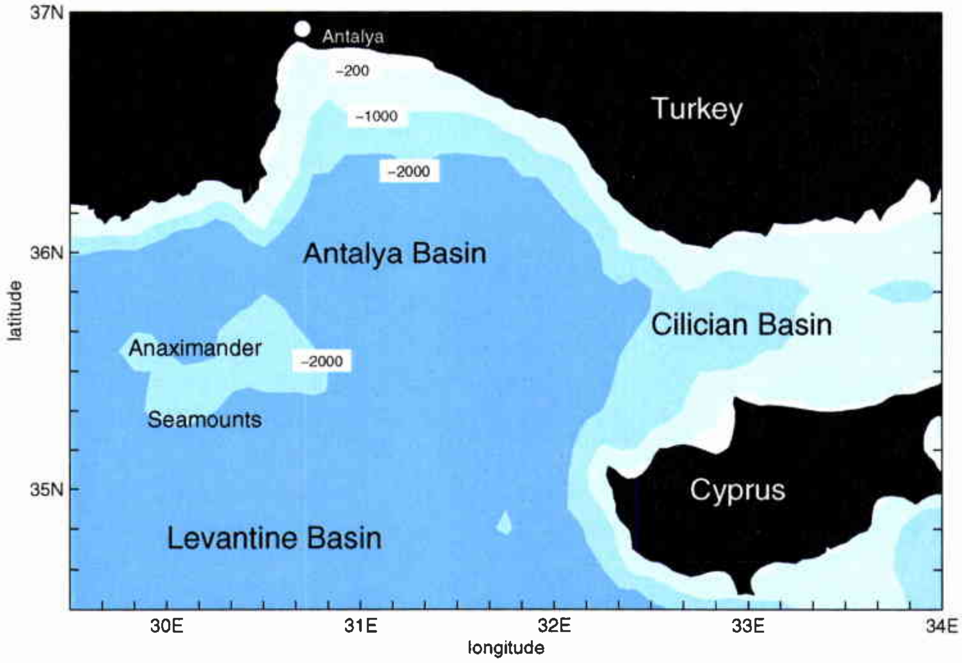

Figure 1 *The Antalya Basin. Water depths are in metres.*

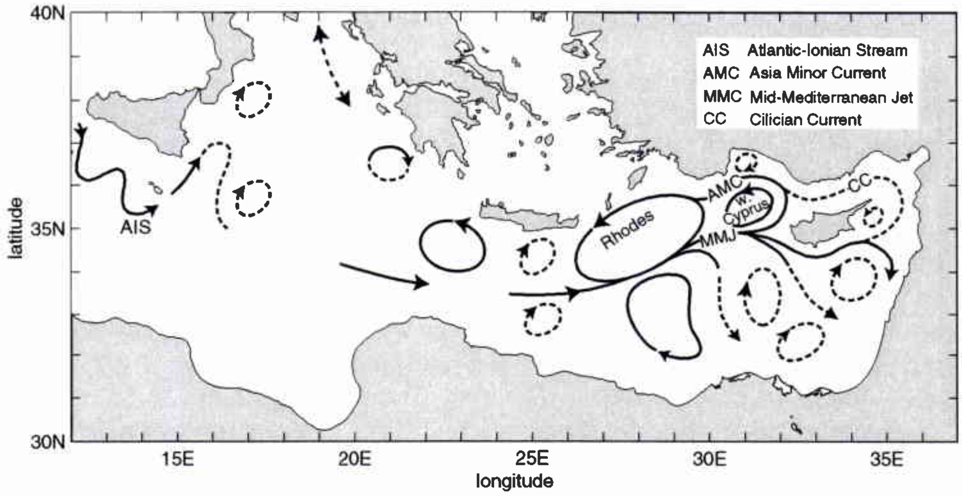

Figure 2 *Schematic upper ocean circulation of the eastern Mediterranean (after [1]).*

net gain of buoyancy, because the heat flux from the atmosphere into the ocean is positive ([5]) overcompensating for the buoyancy loss due to the increase of surface salinity. In winter, the overall buoyancy flux is negative, leading to convection extending primarily to intermediate depths of a few hundred metres. The convectively transformed water mass is referred to as Levantine Intermediate Water (LIW) which is subsequently injected into the main thermocline at intermediate depths around 200 m, from which it can be traced throughout the Mediterranean by means of its salinity maximum. The pathways within the eastern Mediterranean are however relatively unkown and contradictory. Up to now, the process of LIW formation is only partly understood. It is clear that it is initialized by favourable atmospheric conditions causing rapid buoyancy loss of surface waters due to enhanced flux of sensible and latent heat and freshwater. In the Levantine Basin, such conditions occur frequently in winter as a result of strong, cold, dry, northerly "Poyraz" winds from the Taurus Mountains of Anatolia. For many years it was believed that LIW is predominantly formed by deep mixing events around Rhodes ([6]). [7] found direct evidence for LIW formation in the centre of cyclonic eddies between Rhodes and Cyprus. A secondary source region where LIW may be formed in winter, was located by [8] in the southern Levantine Basin close to the coast of Egypt. Further LIW formation sites were identified by [9] and [10] in the Aegean Sea north of Crete and by [9] in the Antalya Basin. [10] were able to show that LIW is formed by vertical mixing along the Cretan shelf and at the periphery of a cyclonic eddy. The mixed water then descends along isopycnals and accumulates in the centre of a neighbouring anticyclone. [9], however, found well-mixed homogeneous water bodies with LIW characteristics in the centre of anticyclones from the surface to depths of about 300 m. The latter study reveals for the first time that anticyclonic eddies play a special role in the formation and transformation process of LIW. On the one hand, they are acting as recipients of LIW formed in neighbouring cyclonic eddies, and on the other hand, convection to intermediate depths occurs also in the centre of anticyclones. In both cases, LIW becomes trapped within the anticyclones and is not instantly spread within the thermocline.

In this paper the hydrographic situation of the Antalya Basin is described as derived from the survey in February 1997. An anticyclonic eddy occupying the central part of the Basin is investigated in greater detail, emphasizing the role of anticyclones in the LIW formation process. The data of the survey and processing methods are described in Section 2, Section 3 contains the results and Section 4 the discussion and conclusions.

2

Data and methods

In February 1997, a high resolution hydrographic survey of the Antalya Basin was conducted by the NATO research vessel *Alliance* and the Turkish vessel *Çubuklu*. The survey consisted of two legs. Leg 1 from February 8–13 was dedicated exclusively to physical oceanography. This leg was divided into surveys, February 8–11 (leg 1/1) and February 11–13 (leg 1/2). The purpose of leg 1/1 was to assess large scale hydrographic conditions, to determine the large scale circulation pattern and to identify locations of intermediate depth convection. Leg 1/2 was essentially a repeat survey of leg 1/1 with the intention of investigating temporal changes. The major objectives of leg 2 (February 16–22) were related to acoustics research, which will not be described, although data from oceanographic measurements will be used.

2.1 Measurements

CTD (Conductivity-Temperature-Depth) profiles were obtained from both vessels using a Neil Brown Mark III CTD on *Alliance* and a Sea-Bird SBE19 CTD on *Çubuklu*. The nominal spacing between individual CTD profiles on leg 1 was 20′(≈30 km) east-west and 10′(18.5 km) north-south (Figure 3). The lower meridional spacing was choosen in order to resolve better the AMC, the flow direction of which is supposed to be predominantly east-west. All CTD casts were limited to a maximum depth of 1000 m, because we were only interested in physical processes at shallow and intermediate depths. The CTD raw data of both CTDs were processed applying standard procedures and the data were interpolated on 1-dbar vertical intervals. The values of a CTD cast nominally located at (36°00′N, 31°10′E) during leg 1/1 were excluded from further analysis, because of unreliable temperature values caused by a malfunctioning of the temperature sensor. Salinity bottle samples and reversed thermometer measurements were taken at the surface and at the deepest depth of each *Alliance* CTD cast for post-cruise calibration. As no such measurements were taken by *Çubuklu*, two intercomparison CTD stations were occupied nearly simultaneaously by both vessels during leg 1/1 (Figure 3). As, based on these comparisons, the *Çubuklu* salinities were too low, a salinity dependent correction was applied according to the empirical formula $S_{Cub} = S'_{Cub} + P(S'_{Cub})$. Here, S'_{Cub} is the original *Çubuklu* salinity, S_{Cub} the corrected *Çubuklu* salinity, and $P(S'_{Cub})$ a third order polynomial fit of the difference between the *Çubuklu* and *Alliance* salinity on the intercomparison stations yielding a perfect match with the *Alliance* salinity (Figure

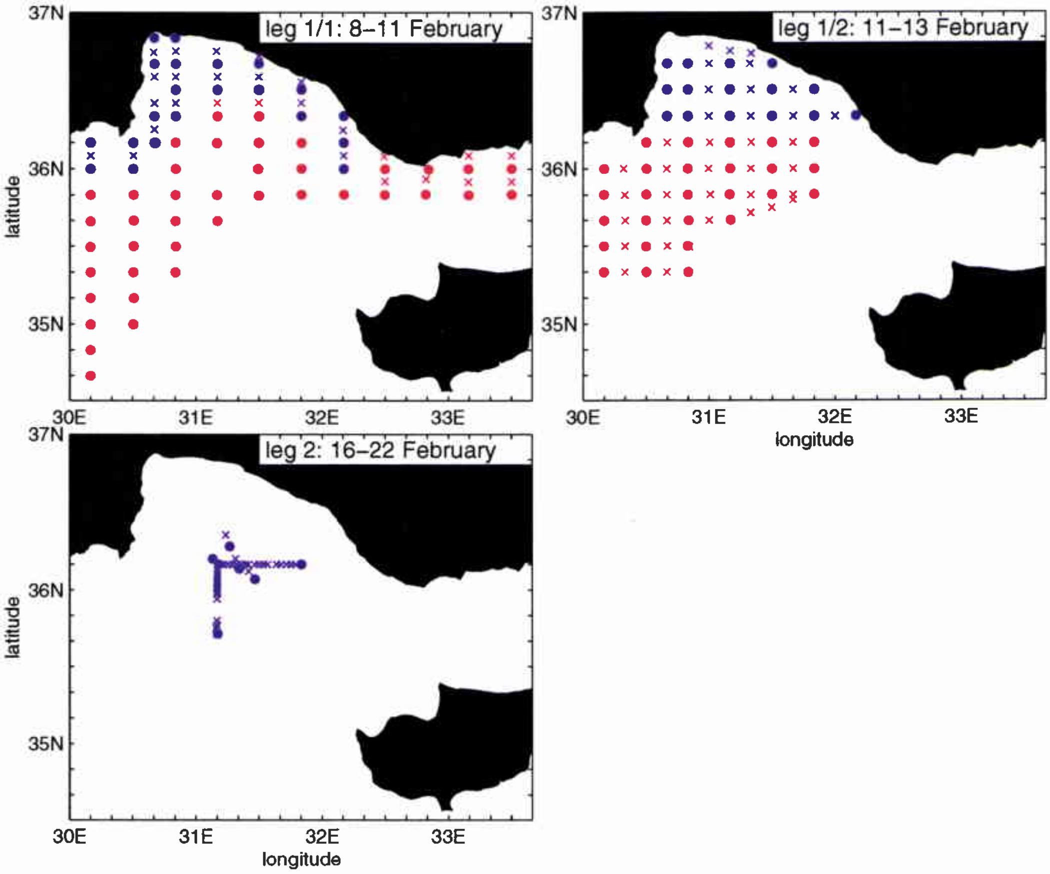

Figure 3 *Positions of Alliance (red) and Çubuklu (blue) CTD stations (dots) and XBT launches (crosses) on legs 1/1, 1/2, and 2. The two CTD stations at (36° 10′ N, 30° 40′ E) and (36° 00′ N, 32° 10′ E) on leg 1/1 were occupied nearly simultaneausly by both vessels for comparison of the CTDs.*

4). The above correction reduced the rms error between the *Çubuklu* and *Alliance* salinity by an order of magnitude from approximately 0.037 to 0.005 psu.

In order to increase the horizontal resolution, XBT (expendable bathythermograph) probes were launched in regions, where the water depth was less than 2000 m on leg 1/1, and at half the zonal distance between CTD stations on leg 1/2. On leg 2, a high resolution XBT survey was carried out along 36°10′N and 31°10′E on February 17 and 18 for support of the acoustic measurements. On *Alliance*, water temperature and salinity at 6 m depth were recorded in 10 minute intervals by a thermosalinograph and water currents were recorded by a ship-borne ADCP (Acoustic Doppler Current Profiler). The raw data were corrected using DGPS (Differential Global Positioning System) navigation data and averaged over 10 min. AVHRR (Advanced Very High Resolution Radiometer) infrared images of the sea

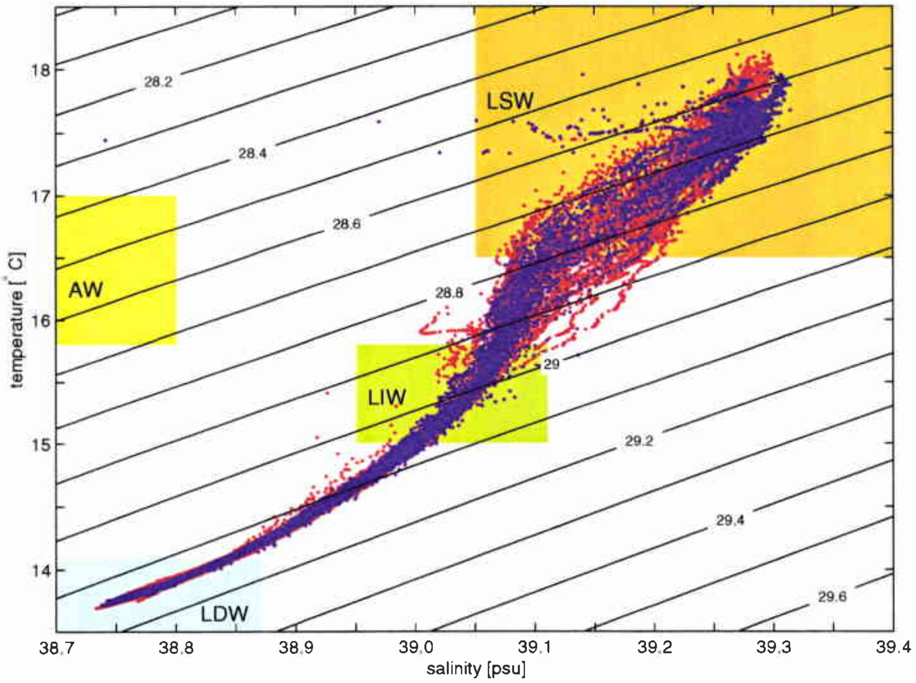

Figure 4 *T/S diagram of all Alliance (red) and Çubuklu (blue) CTD casts after correction of Çubuklu salinity. Contours are lines of constant* σ_t *[kg* m^{-3} *]. Colour shading indicates the temperature/salinity ranges of water masses according to Table 1. For abbreviations see Table 1 and the Glossary section.*

surface temperature were received onboard from satellites NOAA12 and NOAA14 several times per day, and meteorological observations were carried out from the bridge of *Alliance* every 6 hours.

2.2 *Objective analysis*

A 2-dimensional objective analysis scheme ([11]) is used at any instant, when irregularly spaced quantities are mapped on horizontal (isobaric) or quasi-horizontal (isopycnal) surfaces. This scheme performs a linear estimation of any scalar field Φ and the error variance $\epsilon(\Phi)$ at the geographical coordinates (λ, φ) from observational data Φ_{obs} located at $(\lambda_{obs}, \varphi_{obs})$ by using minimum error variance methods. A Gaussian isotropic spatial correlation with length scale L is assumed. As additional input parameters the routine requires an observational error ϵ_{obs} and a parameter ϵ_{clim}, the latter being a measure of the variability of the background climatology.

For all computations described below, a longitude/latitude (λ, φ) grid with horizontal resolution $\Delta\lambda = \Delta\varphi = 0.05°$ is used. $\overline{\Phi_{obs}}$ is the mean value of all observational values Φ_{obs}. It represents the background climatology, which is subtracted prior to the calculation from Φ_{obs} and added to the analysed scalar fields after the calculation in order to obtain Φ. An empirical observational error $\epsilon_{obs} = 0.1 \cdot rms(\Phi_{obs})$ and $\epsilon_{clim} = 10 \cdot \epsilon_{obs}$ are used throughout, where $rms(\Phi_{obs})$ is the root mean square of the observations. A correlation scale L=50 km is used, which is of the order of the length scale of the mesoscale features in this region.

3

Results

3.1 Weather

The weather conditions on all legs are illustrated by time series in Figure 5. Air pressure, wind direction and speed, water and air temperature were measured directly. The relative humidity, the sum of the fluxes of latent and sensible heat, and the freshwater flux have been calculated from the other quantities and the wet-bulb temperature.

During legs 1/1 and 1/2 the weather was calm. The air pressure varied between 1021 and about 1028 hPa, and the wind speed was less than 6 m s^{-1} . The minimum air temperature of about 12°C was recorded at the beginning of leg 1/1 on February 8 increasing steadily to about 16°C in the evening of February 10, and oscillating between 14 and 16°C from then on until the end of leg 1/2. The sea surface temperature fluctuated between approximately 17°C and 18°C, but stayed almost all the time close to 18°C. The relative humidity was between about 40 and and 70%.

On leg 2 the weather was rougher. Between days 16 and 22 the pressure fell almost steadily from about 1024 to 1005 hPa starting to rise again only on the last day. The wind speed was considerably higher and reached a maximum value of nearly 16 m s^{-1} on day 22. In contrast to the previous legs, the air and sea surface temperature reveal a decreasing tendency. The relative humidity fluctuates between about 70 and 90% between days 16 and 21 reaching 100% in the morning of day 21 and decreases to about 50% late on day 23.

A "Poyraz" event is characterized by strong and dry northerly winds causing a rapid buoyancy loss of the near surface ocean layer due to enhanced release of sensible and latent heat. The above records imply that such an event has taken place on the last two days of our survey. There, the wind direction rotated from south over east to north, the wind speed increased to its maximum value and the relative humidity dropped rapidly. The latent and sensible heat flux, which had been less than 160 Wm^{-2} between days 8 and 20, increased to nearly 350 Wm^{-2} at the end of day 23. At the same time, the evaporative fresh water flux increased from its previous value of about 2 to nearly 11 mm day^{-1}. Before, such large values had only been diganosed on day 8 caused by the large air-sea temperature difference and low humidity, not by strong winds.

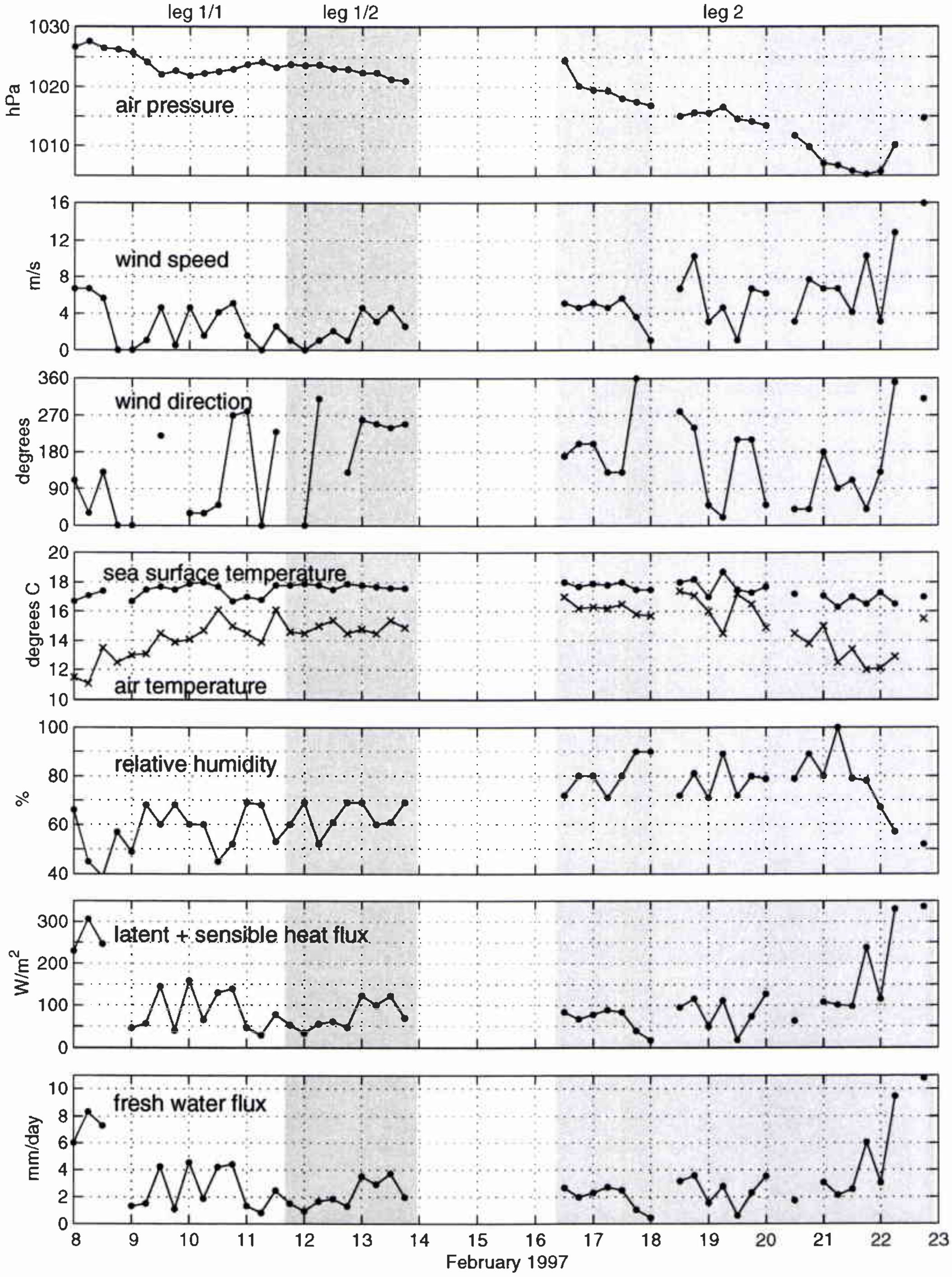

Figure 5 *Time series of meteorological data. The date labels on the time axis correspond to midnight of the respective day. The time coordinate is UTC.*

3.2 Horizontal maps

In the following, maps of those quantities varying with depth will be shown on standard depths of 10, 50, 100, 200, 500, and 900 dbar, where applicable. For the dynamic height and geostrophic flow, the 900 dbar depth is omitted because it is identical with the level of no motion. For the currents measured by ADCP, vertical mean values of the depths ranges 10–50, 50–100, 100–200, and 200–500 m are shown instead, because of the noise in single ADCP profiles and the poor data quality below 500 m. For the distribution of pressure on potential density, the potential density surfaces σ_0= 28.6, 28.7, 28.9, 29.0, 29.15, and 29.17 kg m^{-3} were selected.

3.2.1 Dynamic height and geostrophic flow

The horizontal distributions of dynamic height and geostrophic flow are shown in Figures 6 and 7. The dynamic height was evaluated for each single station using a level of no motion at p=900 dbar and mapped on the regularly spaced grid. No values were provided for stations where the water depth was shallower than the level of no motion. This level of no motion depth was selected for two reasons: similar levels within the 800–1000 dbar range were applied by the majority of previous studies and secondly, 900 dbar is the deepest common level of all CTD profiles not limited by water depth.

The dominating feature of the 10 dbar flow pattern on leg 1/1 is a triangular shaped anticyclonic eddy in the centre of the Antalya Basin — the Antalya Anticyclone (AyAC). Its meridional diameter is approximately 55 km and in zonal direction it extends over nearly 75 km. Maximum currents of 50 cm s^{-1} are found at its southern flank. The eastern half of a second anticyclone (the AxAC) with similar meridional extension and strength of flow is visible at the left edge of the figure. The rest of the Antalya Basin is occupied by cyclonic flow. Three cylones, the centres of which are spaced approximately 100 km apart, are aligned along the southern rim of the survey area. Three weak cyclonic flow patterns encircle the AyAC at its northern periphery. Qualitatively, the flow patterns at the deeper levels resemble closely that at 10 dbar. The strength of the flow, however, decreases from maximum values between 46 and 51 cm s^{-1} in the top 100 dbar range to 3 cm s^{-1} at 500 dbar. Hence, the strongest horizontal density gradients are expected in the 200 to 500 dbar range. In the top 200 dbar, the velocity scales of the AyAC and the AxAC are similar. In contrast, the AxAC velocity is the dominant signal at the 500 dbar level, where the AyAC velocity is considerably weaker. Thus, the AxAC is more depth intensified than the AyAC.

The overall situation found during leg 1/2 is similar, but there are significant changes worth mentioning. The AyAC has changed shape and position, the cylonic flow

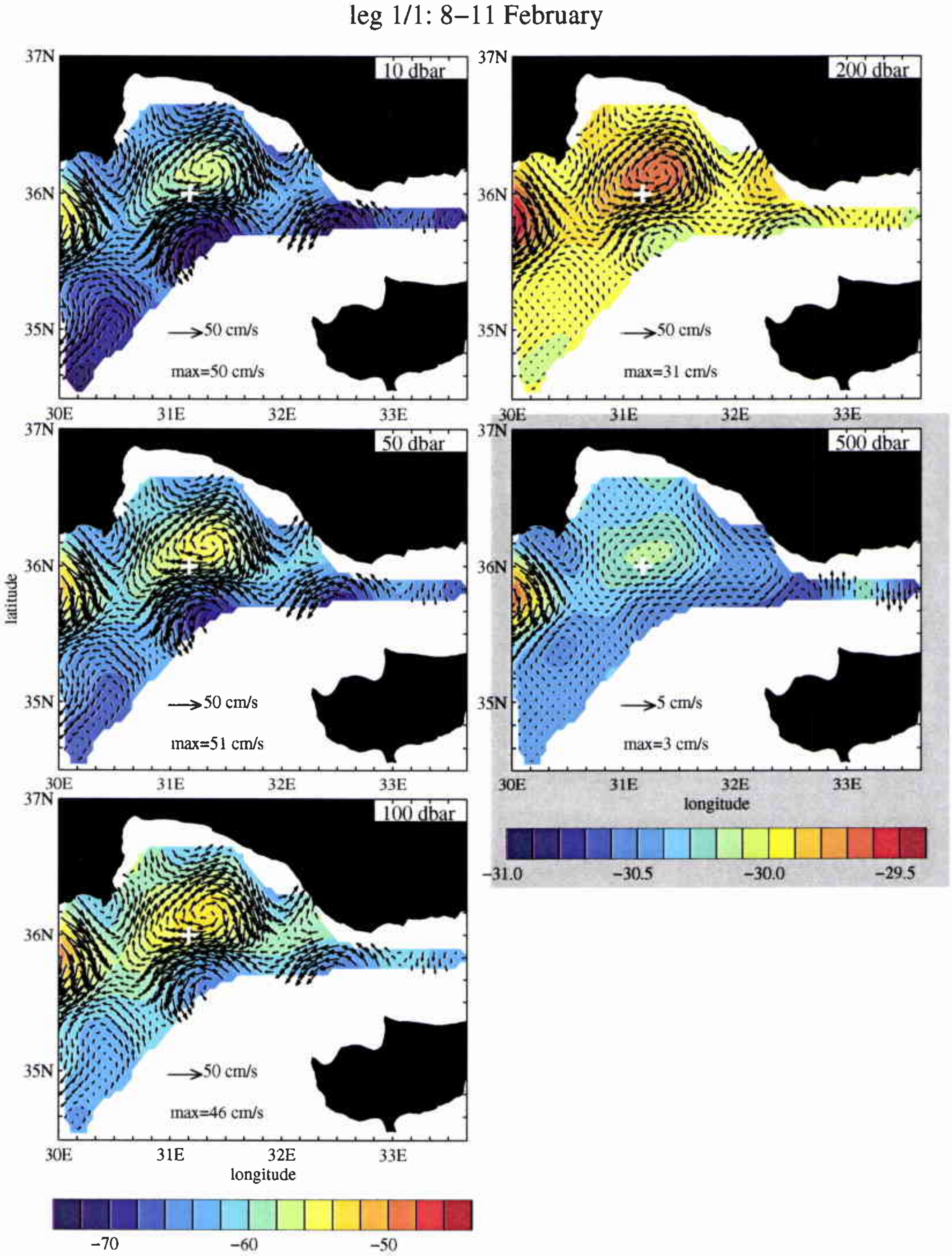

leg 1/1: 8–11 February

Figure 6 *Leg 1/1: Objectively analyzed dynamic height [dyn cm] and geostrophic currents at 10, 50, 100, 200, and 500 dbar relative to 900 dbar. Note the different vector scale, colormap and contour interval at the 500 dbar level. The cross at (36° N, 31° 10′ E) serves as a visual aid to track the motion of the centre of the AyAC and corresponds to the position of the meridional sections in Figures 22 - 27.*

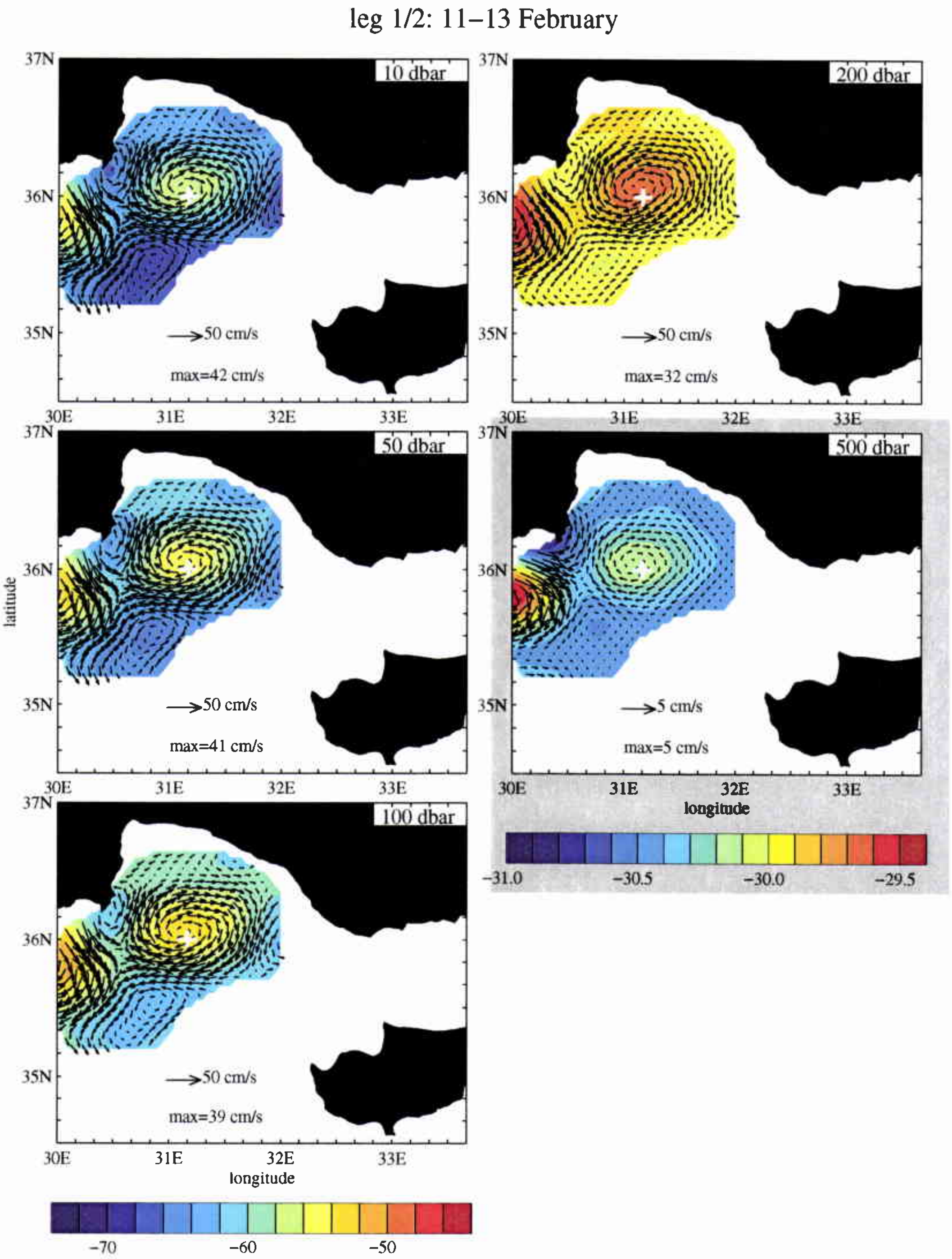

Figure 7 *same as Figure 6, but for leg 1/2*

patterns at the southern rim have been shifted in phase, and the velocity magnitude is different. The shape of the AyAC is more ellipse-like and the centre migrated by about 20 km to the southwest at all levels (equivalent to a phase speed of nearly 7 cm s^{-1}). The cyclonic eddies previously centred at about 30°30′E and 31°20′E have disappeared and a cyclonic eddy is found at 30°50′E. It is conjectured that this cyclone is identical to the one further east during leg 1/1, which travelled to the southwest at a mean speed of about 10 cm s^{-1} . The maximum speeds at 10, 50, and 100 dbar are weaker than during the previous leg, they are at about the same strength at 200 dbar and stronger at 500 dbar. This indicates that a significant fraction of the sear surface kinetic energy was transferred to deeper levels.

3.2.2 Currents from ADCP

For comparison with the geostrophically calculated currents, directly measured currents by ADCP are displayed in Figures 8 and 9. As only *Alliance* was equipped with this instrument, there are no data in the near-shore regions surveyed by *Çubuklu*. However, the ADCP data provide information in areas where the water depth is less than 900 m and no geostrophic currents are available. Because single ADCP measurements are rather noisy, the profiles were averaged over the depth ranges 10–50, 50–100, 100–200, and 200–500 m and finally objectively analyzed.

The ADCP current patterns agree well with the geostrophic currents shown before, but the ADCP currents are stronger by about 50%, which is probably due to smoothing of dynamic topography gradients by the objective analysis. It is interesting to note that in the 200–500 m depth range the strongest velocity signal emerges again from the AxAC as in the 500 m geostrophic currents. Hence, this feature is obviously not caused by a bad choice of the level of no motion.

From both the ADCP and geostrophic currents, there is evidence for the CC meandering westward along the Turkish coast and joined by cyclonic eddies on its southern flank. A continuous AMC is hardly detectable, but one might attribute the flow at the southern flank of the AyAC and AxAC to this feature. During leg 1/2, there is more indication that this could be the approximate flow path.

3.2.3 Volume transport

The geostrophic volume transport is shown in Figure 10 by means of its streamfunction. A different method was applied for the evaluation of the geostrophic flow yielding also information in regions where the water level was shallower than the level of no motion: In situ density was objectively analyzed in 10 dbar vertical intervals between 900 dbar and the sea surface. The geostrophic flow and transport were

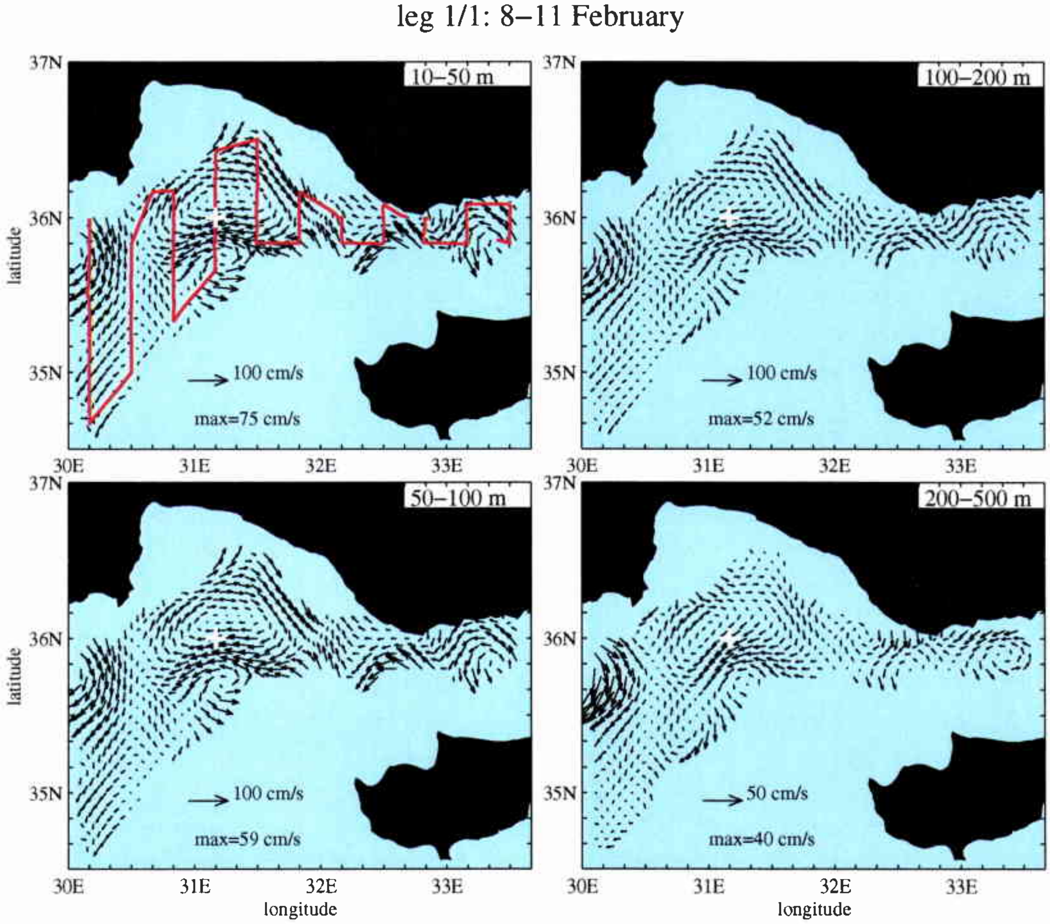

Figure 8 *Leg 1/1: Objectively analyzed mean currents [cm s^{-1}] measured by ADCP for the depth ranges 10–50, 50–100, 100–200, and 200–500 m. Note the different vector scale of the 200–500 m depth range. The red line indicates the ship's track of Alliance.*

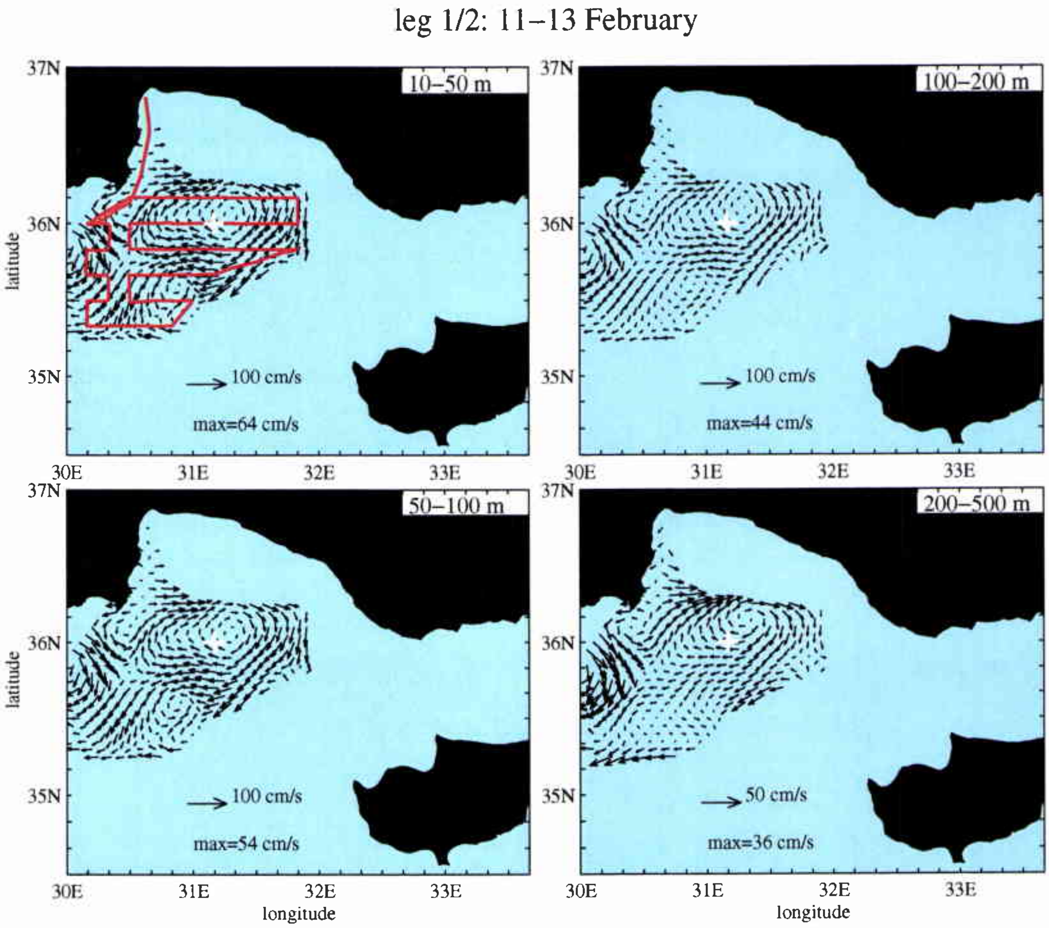

Figure 9 *Same as Figure 8, but for leg 1/2.*

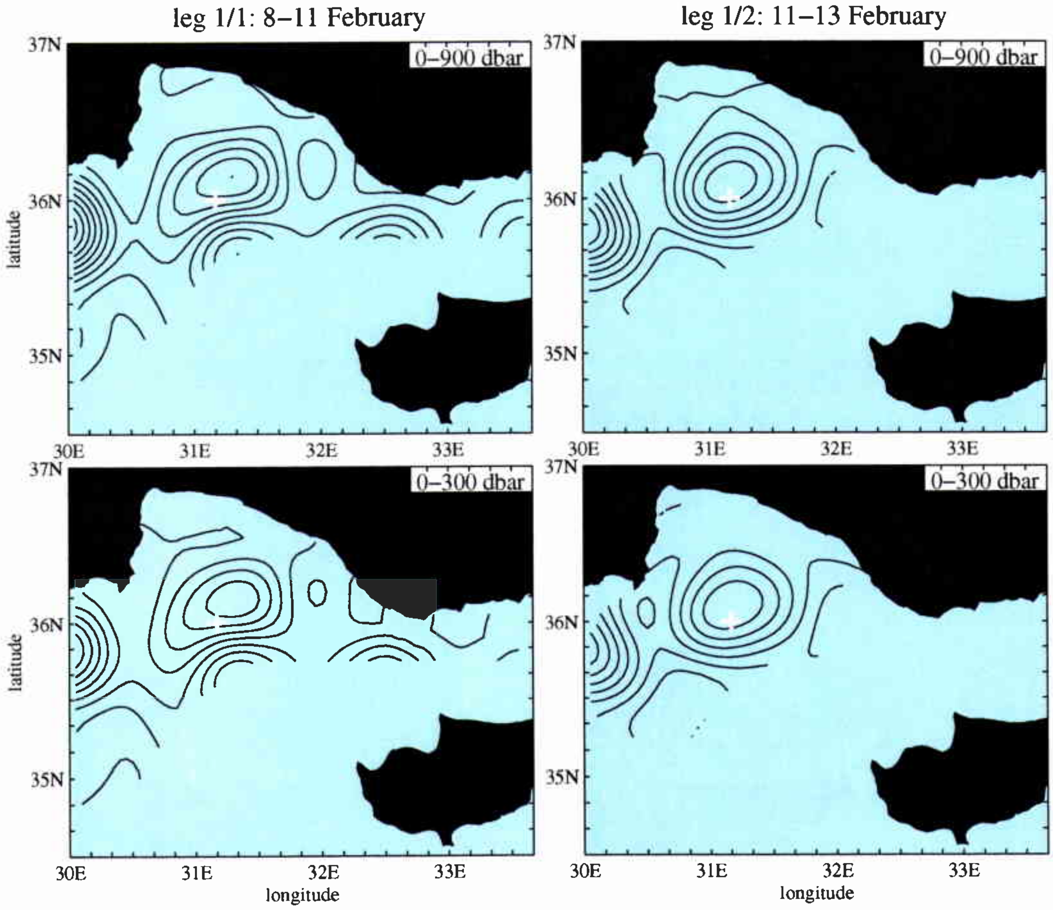

Figure 10 *Volume transport streamfunction [Sv] for the vertical range 0–900 and 0–300 dbar on leg 1/1 and leg 1/2. The transports were integrated relative to 900 dbar. The transport between adjacent contours is 0.5 Sv.*

computed for every 10 dbar layer using the thermal wind equation. As the objective analysis scheme does not take into account the bottom topography, transport values were set to zero below the bottom using the ETOPO5 bottom topography ([12]). The transport was integrated vertically between the sea surface and 900 and 300 dbar, respectively.

As the resulting structures in the 0–900 dbar range reveal strong similarities with the geostrophic flow shown before, it can be concluded that the flow patterns identified from Figures 6 and 7 are coherent over the entire 900 dbar depth range. On leg 1/1, the AyAC and AxAC are again the dominating features exhibiting volume transports of 2 and 3 Sv (1 Sv= $10^6 m^3 s^{-1}$), respectively. The three cyclones at the southern rim of the survey area are weaker, their transport is less than 1.5 Sv, and the transport of the cyclones located to the north and east of the AyAC does not exceed 0.5 Sv. On leg 1/2, the AyAC has also attained a more circular shape and its centre shifted westward. The three southern cyclones obviously moved westward with the westernmost one having left the survey area. There is evidence that parts of the cyclone, which is now centred at about (35°25′N, 30°45′E), are sucked northward by the flow around the AyAC and may eventually be advected towards the coast.

The streamfunction pattern for the 0–300 dbar range is rather similar to that of the 0–900 dbar range. The transport of the AxAC and AyAC is only slightly weaker, which is another indication that the current pattern is mainly baroclinic and significant transport occurs only in the upper about 300 dbar range.

3.2.4 *Potential density*

Figures 11 and 12 show the distribution of potential density on standard pressure levels. At 10 and 50 dbar on leg 1/1, a well defined front runs across the survey area from southwest to northeast. Another frontal zone oriented parallel to the Turkish coast becomes visible at 100 dbar depth east of 32°E, and the 200 dbar density distribution reveals clearly that both frontal zones are connected. They indicate the flow path of the CC and the AMC and will be referred to as the AMC front. At 500 and 900 dbar, the front is hardly detectable, which confirms the earlier finding that the major current system is confined to the upper about 300 dbar.

The horizontal density differences at 10 and 50 dbar are weak and do not exceed 0.5 kg m^{-3} . Low density is approximately correlated with anticyclonic flow (cf. Figure 6) and higher density prevails at locations where cyclonic eddies were diagnosed above. Qualitatively, the density at 100 dbar looks rather similar, but the density differences are stronger than at 10 and 50 dbar. This is primarily due to higher density in the cyclonic eddies, whereas the density in the AxAC and AyAC is about the same as at the levels above. Hence, the near surface stratification is weak in the anticyclones and strong in cyclonic eddies. The strongest density differences of nearly 1 kg m^{-3} occur at 200 dbar. The density contours are highly correlated with the dynamic height of the layers above, which means that the major contribution for the vertical geostrophic shear comes from this depth range. The major density anomaly at 500 dbar agrees with the position of the AxAC. Here, the density is about 0.05 kg m^{-3} less than the background field. In contrast, the negative anomaly caused by the AyAC is less than half of that, which is a further indication for the depth intensification of the AxAC. At the 900 dbar level, density differences are generally less than 0.01 kg m^{-3} , and only the AxAC becomes visible with the selected contour interval.

Comparing the density at the top four pressure levels on leg 1/2 with the respective distributions on leg 1/1 confirms the previously diagnosed pattern changes. This is the change of shape and the westward migration of the AyAC and the translation

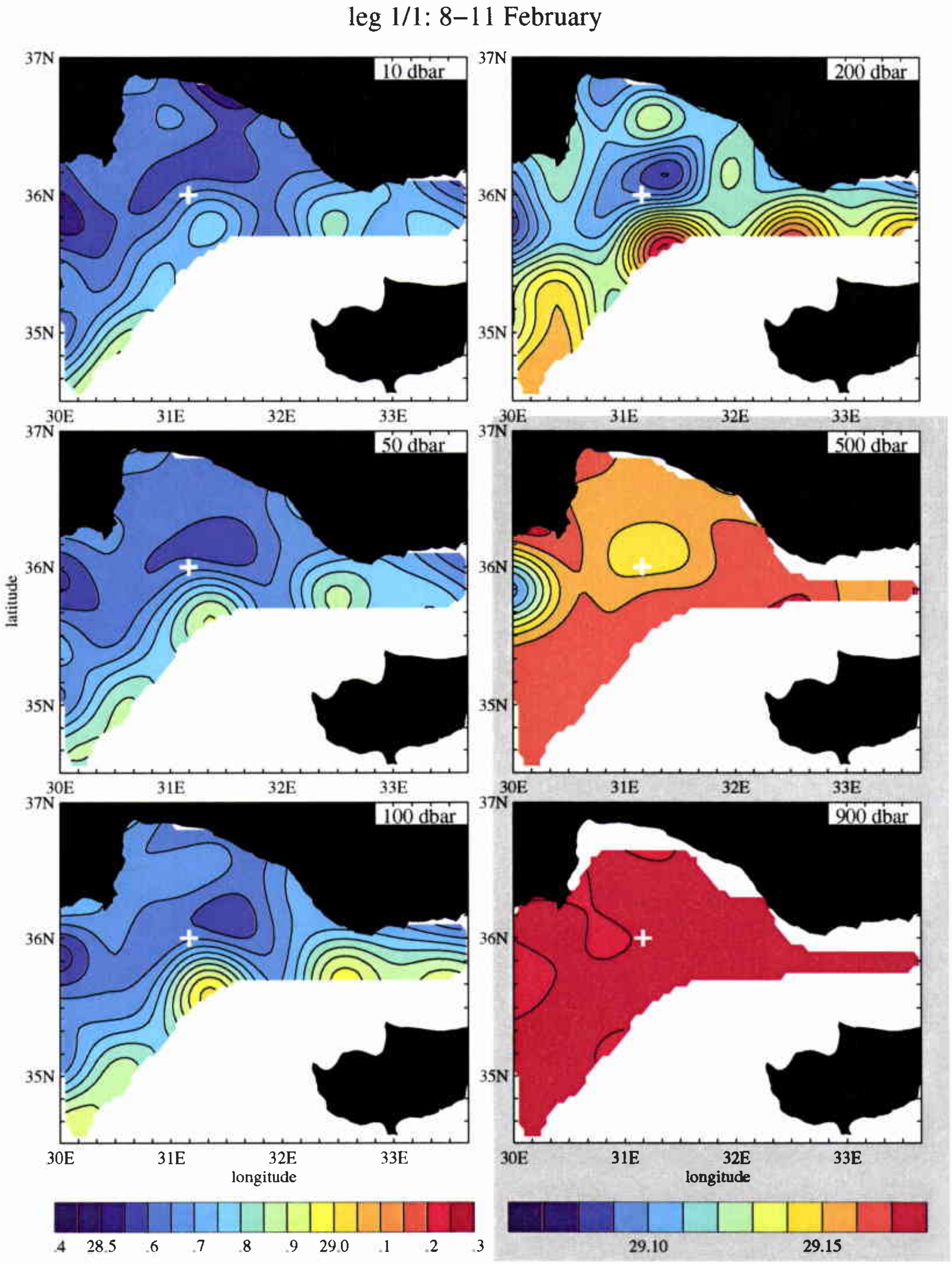

Figure 11 *Leg 1/1: Objectively analyzed potential density [kg* m^{-3} *] at 10, 50, 100, 200, 500, and 900 dbar. Note the different colormap and contour interval for the 500 and 900 dbar pressure levels.*

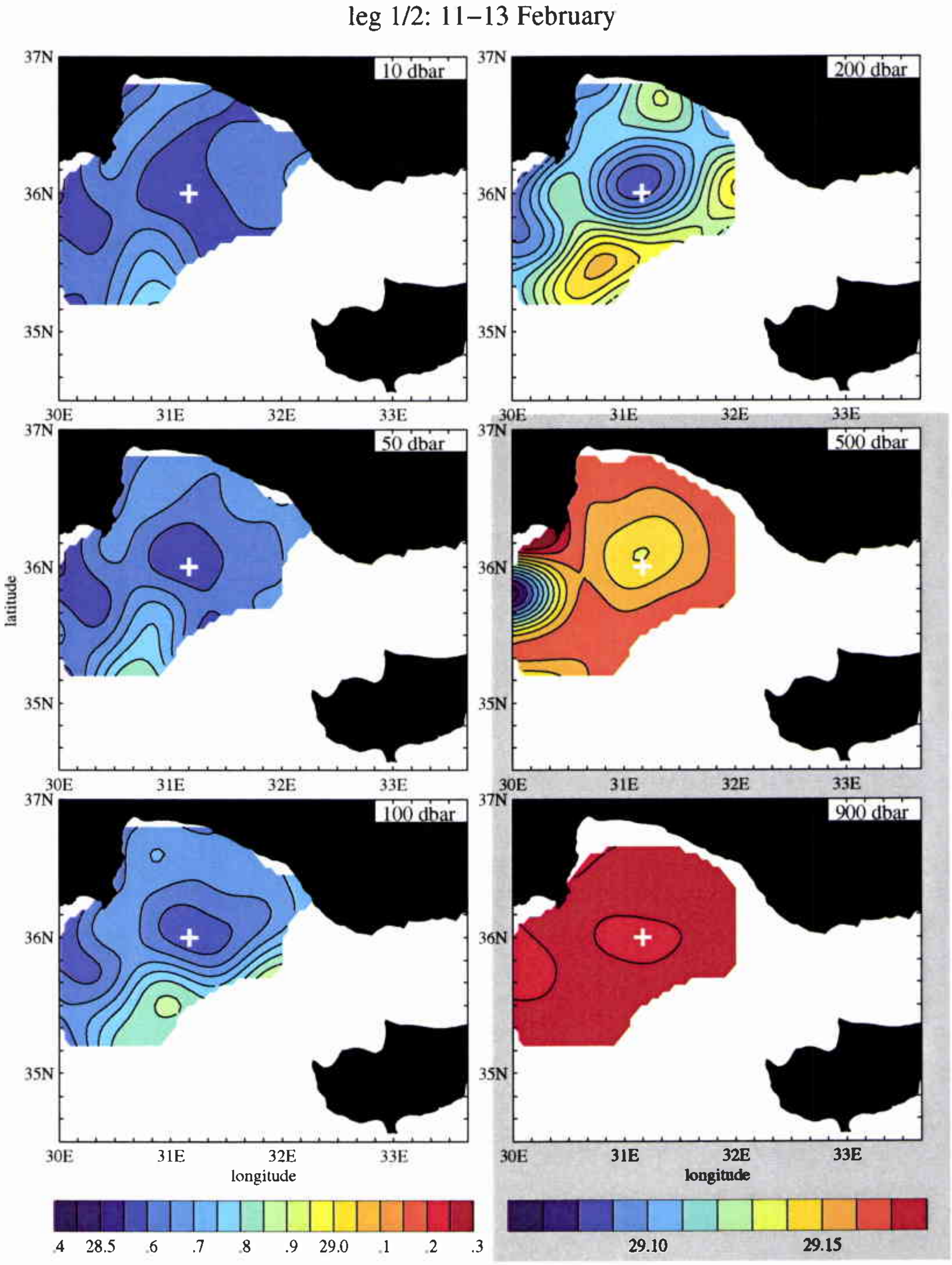

Figure 12 *Same as Figure 11, but for leg 1/2.*

of the AMC meanders. The growth of a meander trough is clearly visible by means of a high density lobe extending northward between the AxAC and the AyAC. At 500 dbar, the density contrast with the background field of both the AxAC and the AyAC did increase, and also at 900 dbar the AyAC becomes visible suggesting again a downward directed transfer of kinetic energy.

3.2.5 Pressure on potential density

It is useful to evaluate distributions of physical quantities on surfaces of potential density σ_0, because the large scale flow in the oceans is believed to be predominantly isopycnic, i. e. along surfaces of $\sigma_0 = const.$ Presenting the distribution of pressure on potential density provides additionally information on water mass formation processes by tracing back the respective isopycnals to their outcrop locations at the sea surface.

Pressure on σ_0 for six selected isopycnals is shown in Figures 13 and 14 for legs 1/1 and 1/2. $\sigma_0 = 28.6$ kg m^{-3} is the isopycnal next to the sea surface, which is only defined in a region north of 35°40′N and west of 32°E on leg 1/1. Everywhere else, the water is denser. Maximum pressure values of more then 200 dbar are found northeast of the centre of the AyAC and more than 250 dbar in the centre of the AxAC. A third high pressure centre is located between the AyAC and the AxAC. Outcrop lines are located along the northwest coast of the Antalya Basin and approximately at the northern rim of the AMC frontal zone. These lines are possible sites of water mass renewal on this density horizon. The next isopycnal, $\sigma_0 = 28.7$ kg m^{-3} , exhibits maximum pressure values of more than 300 dbar in the centre of the AyAC and over 200 dbar in the AxAC. Outcrops are located in the AMC front and approximately along 32°E. $\sigma_0 = 28.9$ kg m^{-3} is the first isopycnal, which can be found over nearly the entire survey area. It extends to maximum depths of more than 300 dbar in the centres of anticyclonic flow and outcrops in the centres of the three cyclones at the southern boundary of the survey area. $\sigma_0 = 29.0$ kg m^{-3} lies below the surface everywhere. Maximum pressure is found again in regions of anticyclonic flow and also in a narrow strip along the Turkish coast. This may be an indication for coastal downwelling. The deepest isopycnals shown are $\sigma_0 = 29.15$ and 29.17 kg m^{-3} . On both isopycnals high pressure can still be identified at the locations of the AxAC and AyAC. The pressure differences on the deeper isopycnal are about twice as large as on the shallower one, which are due to the weaker vertical gradients in this depth range.

Between legs 1/1 and 1/2, major changes occured on all isopycnals. On $\sigma_0 =$ 28.6 kg m^{-3} , the three centres of high pressure merged into two located at the AxAC and AyAC positions. On the deeper isopycnals σ_0=28.6, 28.7, 28.9, 29.0, and 29.15 kg m^{-3} , the earlier mentioned displacement and change of shape of the AyAC becomes visible by a respective translation and reshaping of the high pressure

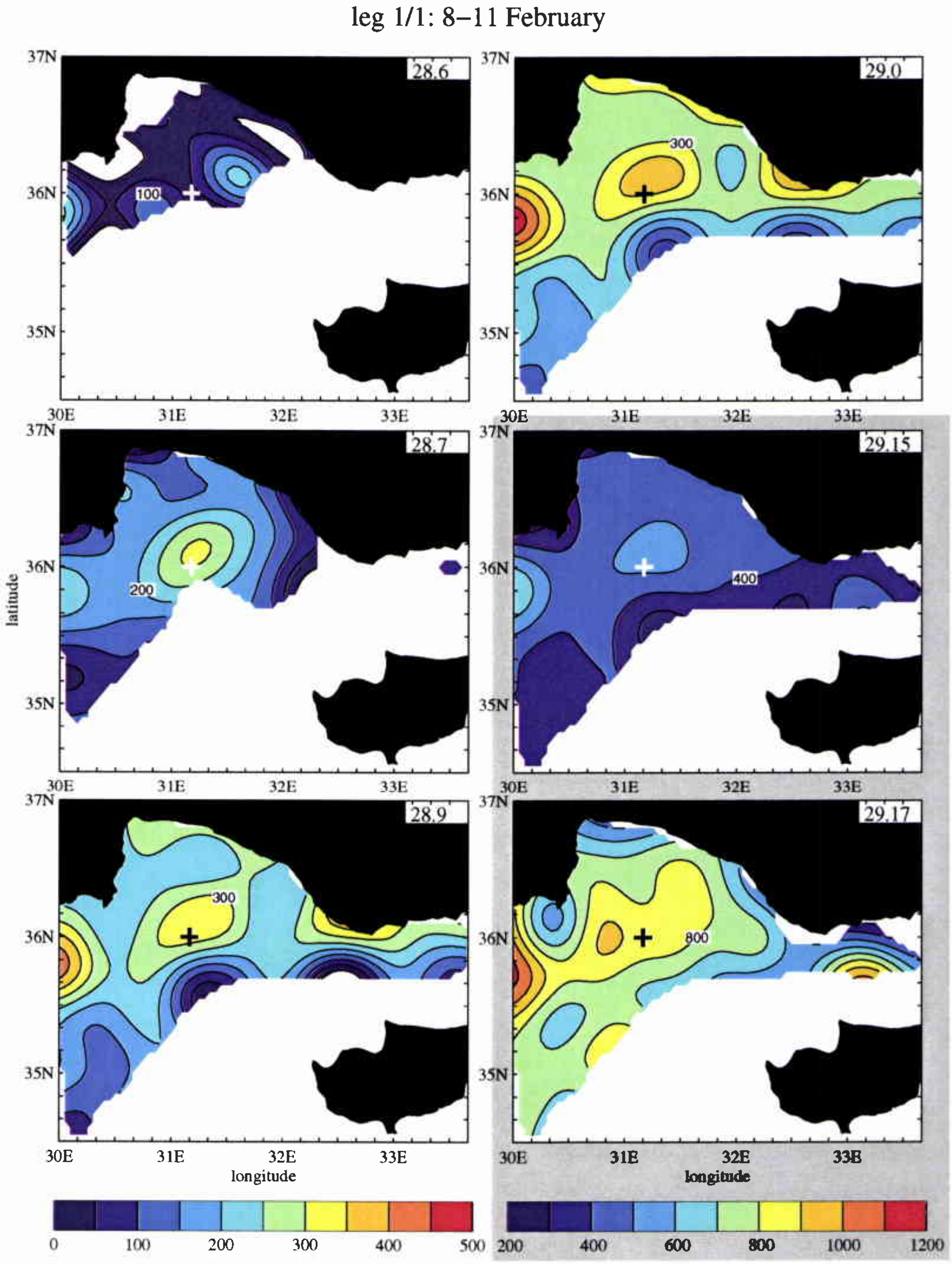

Figure 13 *Leg 1/1: Objectively analyzed pressure distribution [dbar] on potential density surfaces* σ_0*=28.6, 28.7, 28.9, 29.0, 29.15, and 29.17 kg* m^{-3} *. Note the different colormap and contour interval for the 29.15 and 29.17 kg* m^{-3} *density levels.*

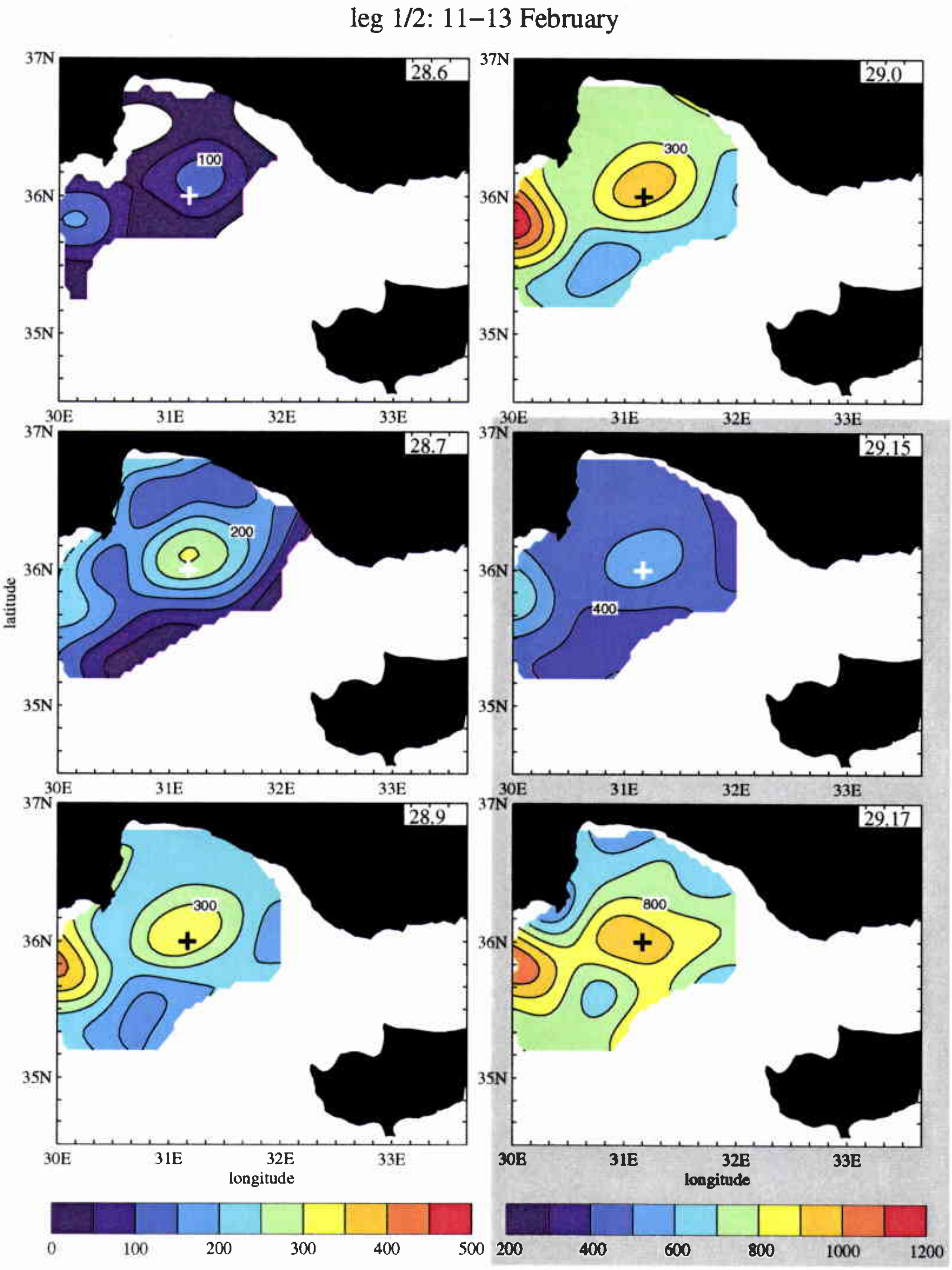

Figure 14 *Same as Figure 13, but for leg 1/2.*

cells. In the same way, the displacement of the AMC meanders is mirrored by the movement of low pressure regions. On the deepest isopycnal, $\sigma_0 = 29.17$ kg m^{-3} , there is indication for a pressure rise at the AyAC location and an increase of the vertical coherence of the pressure field. This supports the ealier finding of the AyAC to become more barotropic.

3.2.6 *Temperature from CTD and XBT*

Horizontal distributions of temperature on standard levels are displayed in Figures 15 and 16. On leg 1/1, the temperature patterns at 10, 50, and 100 dbar exhibit high temperatures in the northern and northwestern region of the survey area with local maxima exceeding 18°C in the AyAC and AxAC on every level. Towards the south and east, temperatures are lower, reaching minimum values around 16°C in the centres of cyclonic eddies. Both regions are separated by the well defined AMC front. At 200 dbar the structures look qualitatively similar, but the differences are larger than in the layers above. In the centre of the AyAC and the AxAC, the temperature is still close to 18°C, hence the anticyclones are characterized by homogeneous pools of warm water, whereas the cyclonic eddies are cold and the stratification in the upper 200 dbar range is stronger. Also at 500 and 900 dbar the anticyclones can still be identified by means of higher temperature, but here the AxAC is warmer than the AyAC, which again supports the observation that the latter is more depth intensified.

Major changes between leg 1/1 and leg 1/2 have occurred in harmony with changes of the dynamics. It is worth to mention that the temperature at 500 dbar decreased in the AyAC, but it increased in the AxAC. Hence, at this level upwelling may have taken place in the AyAC and downelling in the AxAC.

3.2.7 *Salinity from CTD*

Except for the 10, 50, and 100 dbar levels on legs 1/1 and 1/2, the distribution of salinity on standard levels (Figures 17, 18) is highly correlated with temperature. This relationship can already be seen from 4. Salinity maxima are found in the centres of anticyclones and minima in cyclones. The lower correlation in the upper layers is due to the circumstance that the heat and freshwater flux at the sea surface, which finally determines the temperature and salinity, are generally not correlated. Another feature, which can be seen only in the salinity distribution at 10 dbar, are the low values close to the Turkish coast at about 31°30′E caused by fluvial inflow.

Because salinity and temperature are not well correlated near the surface, some important ideas concerning vertical mixing can be drawn from the temporal changes

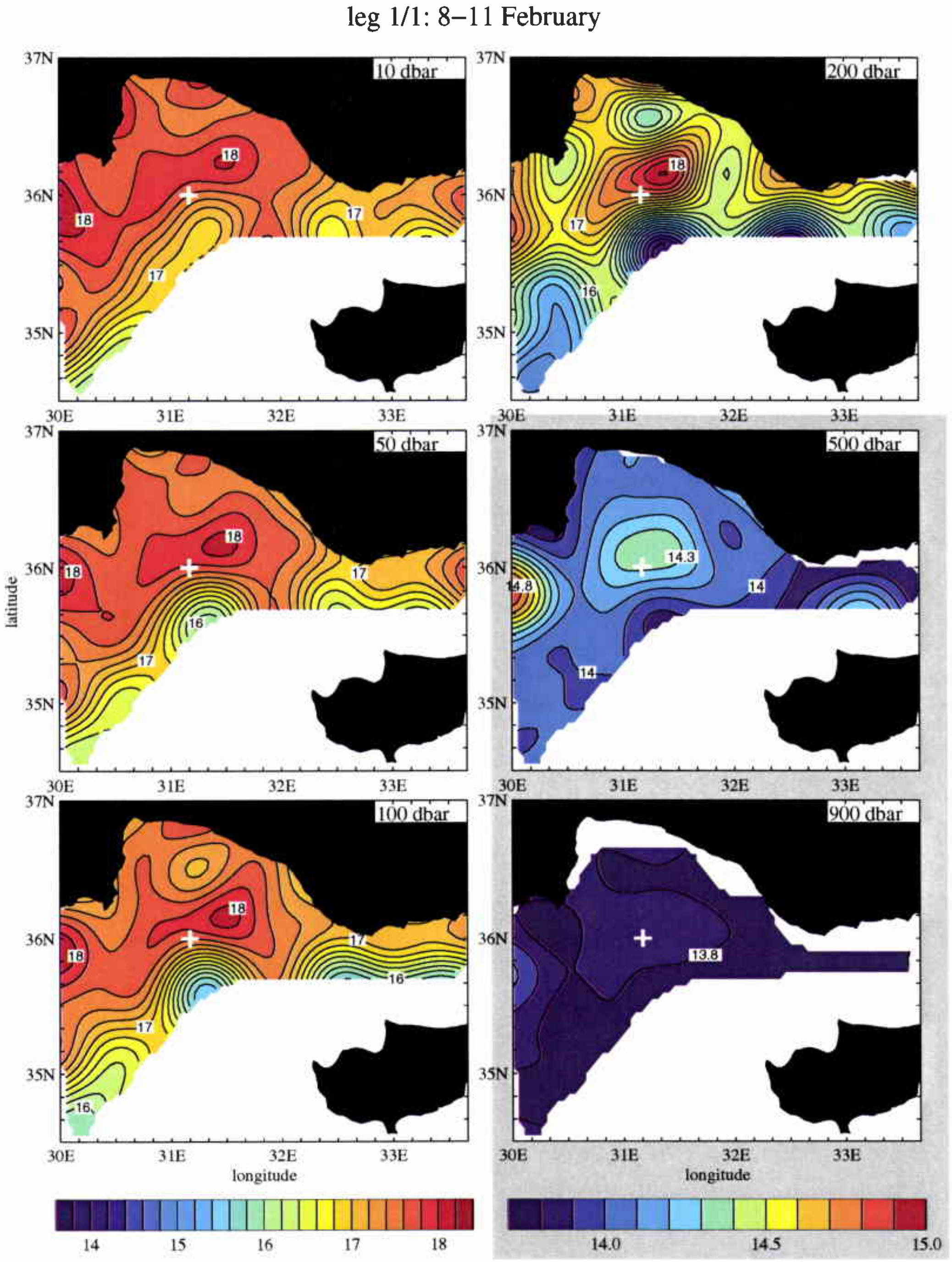

Figure 15 *Leg 1/1: Objectively analyzed temperature [°C] at 10, 50, 100, 200, 500, and 900 dbar. Note the different colormap and contour interval for the 500 and 900 dbar pressure levels.*

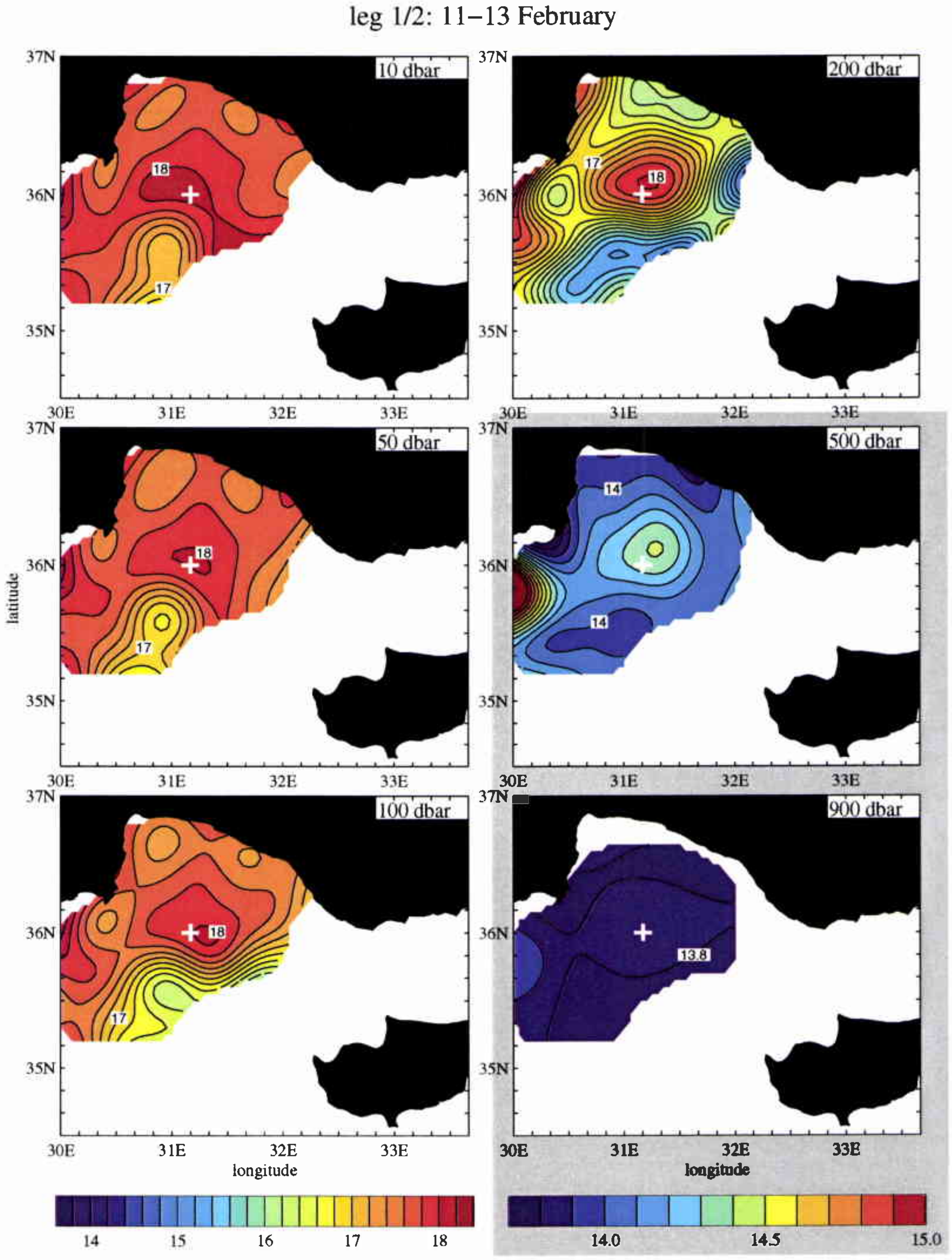

Figure 16 *Same as Figure 15, but for leg 1/2.*

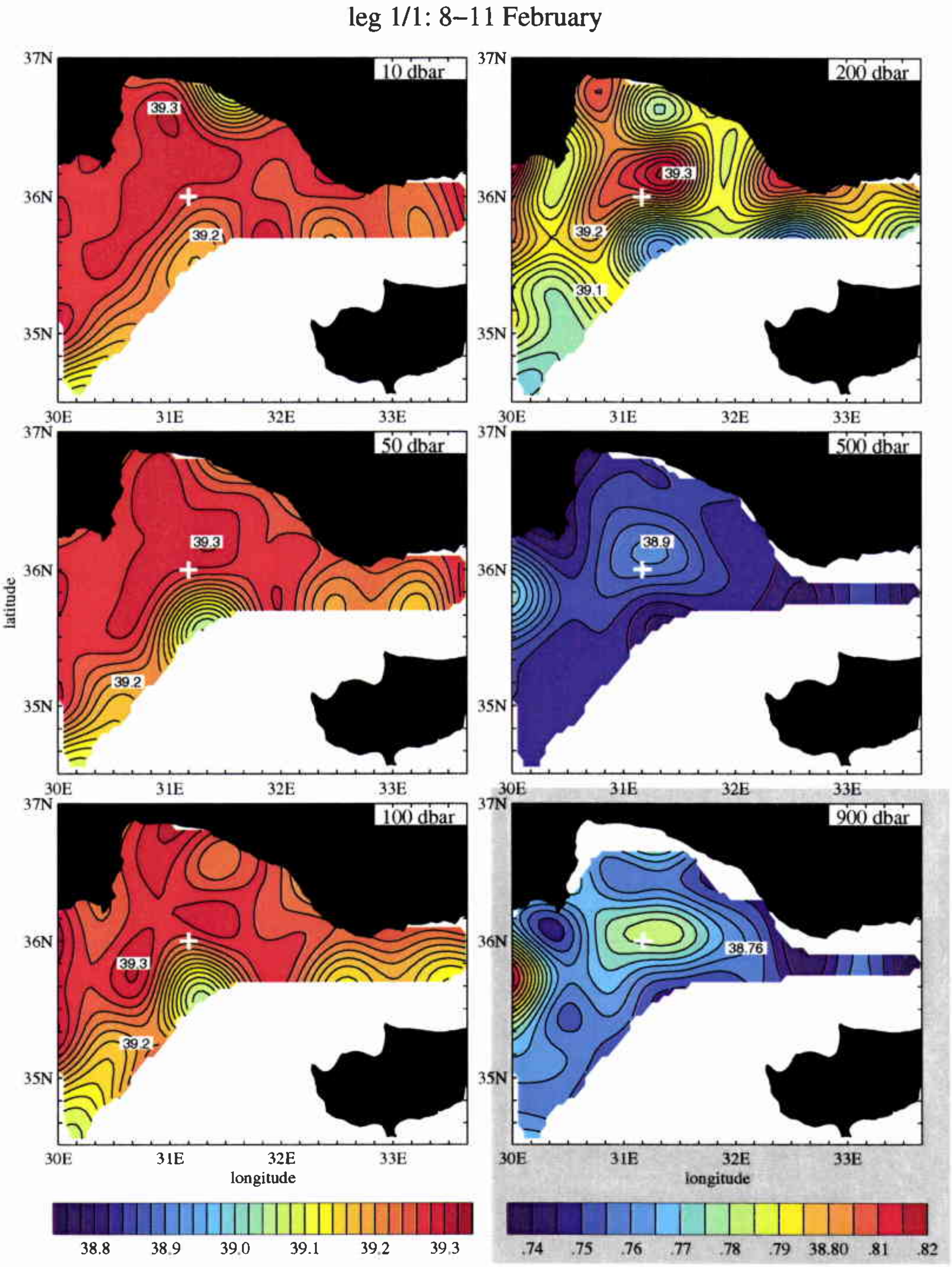

Figure 17 *Leg 1/1: Objectively analyzed salinity [psu] at 10, 50, 100, 200, 500, and 900 dbar. Note the different colormap and contour interval for the 900 dbar pressure level.*

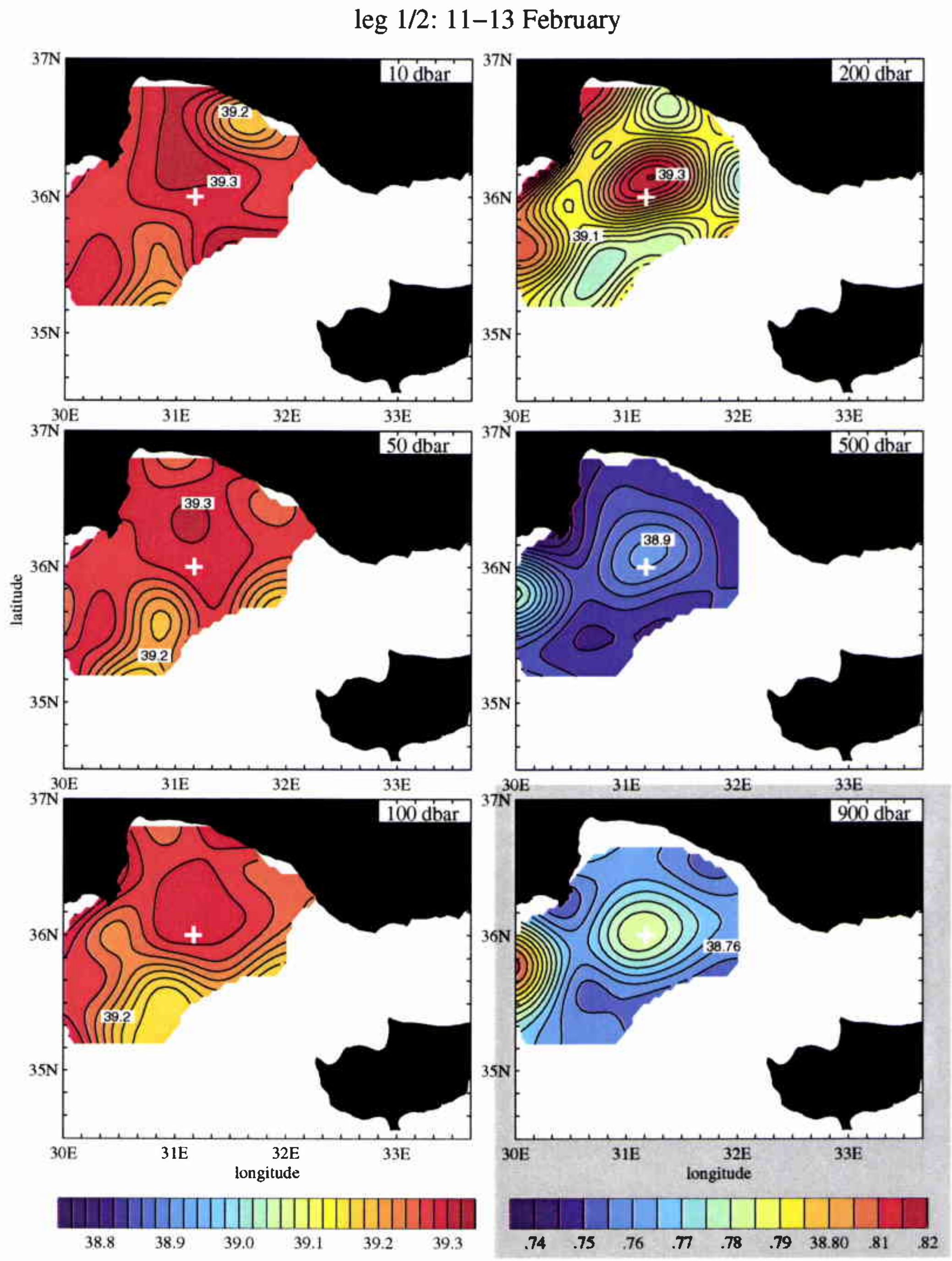

Figure 18 *Same as Figure 17, but for leg 1/2.*

of salinity. In the objectively analyzed fields on leg 1/1, salinities higher than 39.3 psu are found in the northwest corner of the Antalya Basin at 10 dbar, northeast of the cross at 50 and 200 dbar, and southwest of the cross at 100 dbar. However, by re-examining the original CTD profiles, it has been verified that the salinities $\geq$ 39.3 psu at the latter three levels are an artefact of the objective analysis. Only the high salinity $\geq$ 39.3 psu at 10 dbar is supported by a CTD cast, and this cast is the only one on leg 1/1 where salinities $\geq$ 39.3 psu are found, namely between the surface and 53 dbar. In contrast, the salinity exceeds 39.3 psu in four casts on leg 1/2 at stations north of 36°N and around 31°causing the high salinity tongue at 10 dbar and the patch $\geq$ 39.3 psu at 50 dbar. This increase of salinity can only be due to evaporation, the effect of which is difficult to trace in the temperature field.

3.2.8 *Temperature and salinity from thermosalinograph*

Temperature and salinity records of the thermosalinograph on *Alliance* are shown in Figure 19 for legs 1/1 and 1/2. These records provide a good tool for detecting fronts, because they resolve horizontal gradients better than CTD and XBT sampling and no averaging of the data is done as by objective analysis. As the precision of such measurements is generally known to be low, temperature and salinity were compared with CTD values at 10 m depth at the corresponding locations. It turned out that the temperature values were reliable, but salinity exhibited a steady increase with time. Therefore, a linear trend based on the difference between thermosalinograph and CTD salinity was removed.

The temperature and salinity records on leg 1/1 clearly reveal the location of the AMC front, the position of which may be described by the 17.5°C isotherm or the 39.2 psu isohaline. Here, the temperature changes by about 0.5°within two samples and the salinity by 0.1 psu at the same time, which is equivalent to horizontal gradients of about 0.15°C km^{-1} and 0.03 psu km^{-1}, respectively at a ship speed of 10 knots. Also the warm AyAC and AxAC can be identified. On leg 1/2 the northward intrusion of the cold and fresh AMC meander west of 31°E becomes visible.

3.2.9 *Mixed-layer depth*

On legs 1/1 and 1/2, mixed-layer depths are calculated from CTD and XBT profiles using a temperature criterion. For each profile the mixed-layer depth is defined to be that depth, where the difference between the temperature at that depth and the temperature at 5 dbar exceeds 0.5°C for the first time. The objectively analyzed mixed-layer distribution is shown in Figures 20. On leg 1/1, the mixed-layer depth range is from more than 300 dbar in anticyclonic flow regions to zero in the centres

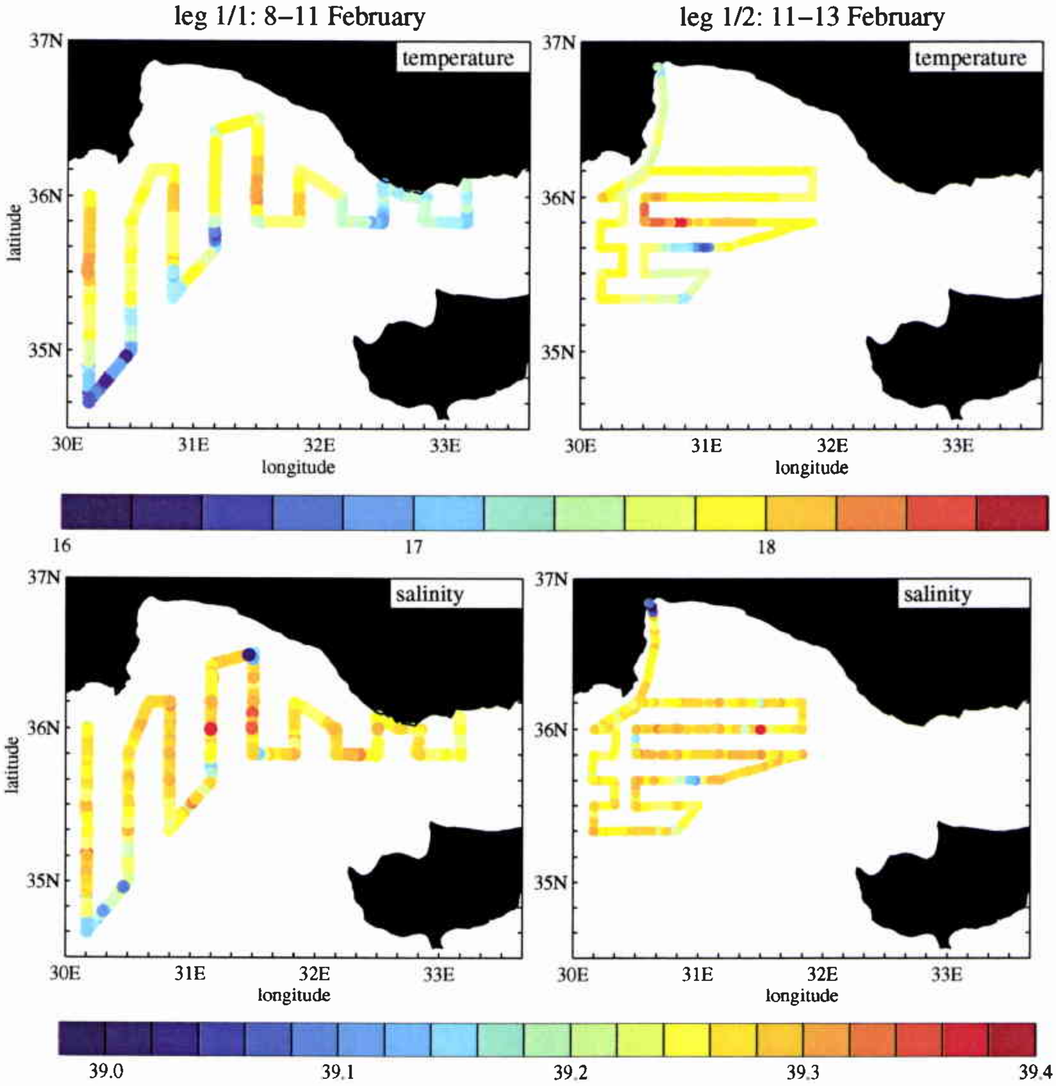

Figure 19 *Temperature [°C] and salinity [psu] at about 6 m depth recorded by the thermosalinograph of Alliance on leg 1/1 and leg 1/2. Every coloured dot refers to a single sample taken in 10 minute intervals.*

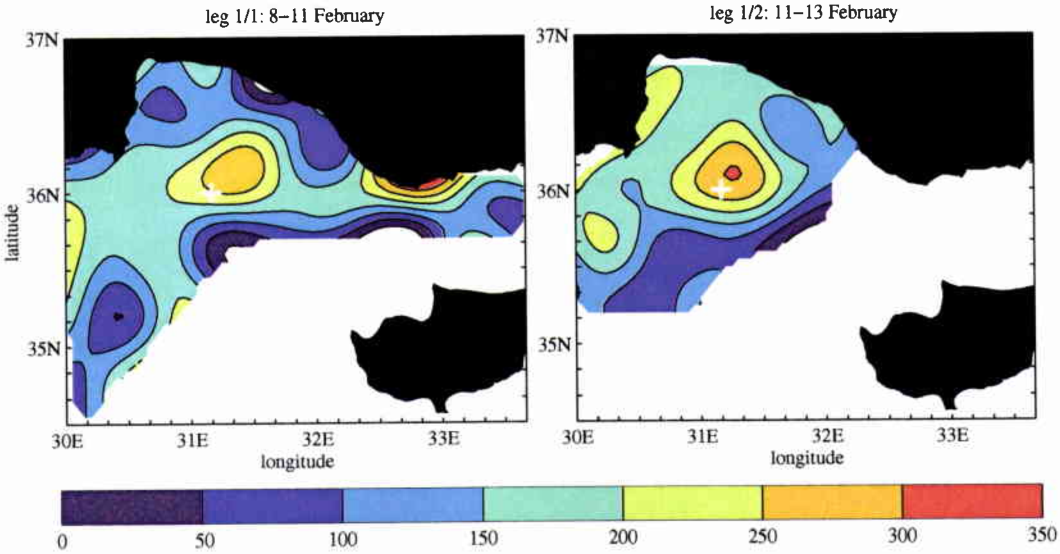

Figure 20 *Objectively analyzed mixed-layer depth [dbar] on leg 1/1 and leg 1/2. For definition of the mixed-layer depth see text.*

of the cyclonic AMC eddies and at the Turkish coast at about 31°30′E. This distribution emphasizes the low stability in regions of anticyclonic and the high stability in cyclonic flow regimes. On leg 1/2, the situation is significantly different. In the AyAC, the mixed-layer depth did increase by about 50 dbar and all along the Turkish coast by 100 dbar or even more. As it is unlikely that the latter dramatic depth changes are caused by atmosphere-driven processes, it is assumed that they are a dynamic response to the translation of cyclonic eddies advected anticyclonically at the periphery of the AyAC.

3.2.10 AVHRR images

AVHRR infrared satellite images of the sea surface temperature (SST) were received several times per day onbard *Alliance*. A selection of six images representative for each day of the survey is displayed in Figure 21. In all images the SST structure exhibits three regimes: relatively warm surface water (≈ 17–18°C) occupies approximately the entire survey area. Another large warm patch is located south of Cyprus. The SST between these two warm water regimes is lower at about 16°C. The boundary between the northern warm water regime and the cold water area exhibits sharp temperature fronts and it is fragmented by lateral intrusions and meanders, the horizontal scales of which cover a spectrum from about 10 to 100 km. From these images and the previously shown shipboard measurements it is concluded that the frontal meanders are identical with the location of the AMC. Hence, the AMC is fed by the CC entering the Antalya Basin by means of a westward meandering current. The

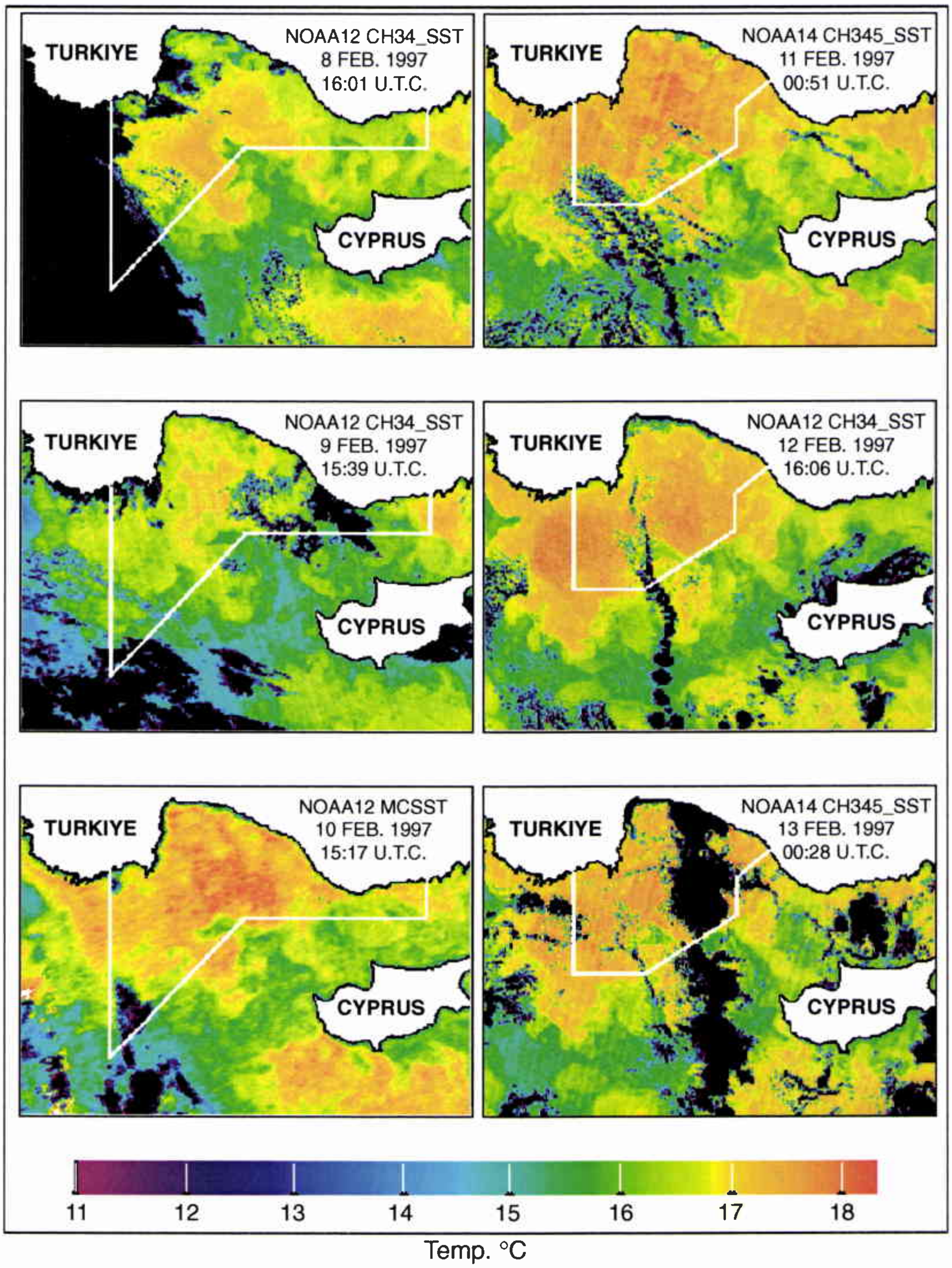

Figure 21 *Infrared images of the sea surface temperature from satellites NOAA12 and NOAA14 in one-day intervals between February 8 and 13. The left panel covers approximately leg 1/1, the right panel leg 1/2. The horizontal area shown extends from 29° E to 34° E and from 34° N to 37° N. In the left panel, the white frame denotes the approximate region of the leg 1/1 hydrographic survey. In the right panel, the corresponding region of leg 1/2 is indicated.*

AMC then takes on a more southwesterly orientation at about 32°E, turns westward again at about 31°E and then northward towards the Turkish coast at about 31°E. Thus, it seems that the AyAC and the AxAC prohibit the AMC to cross the Antalya Basin on the shortest possible way, but to make a detour via a path shifted to the south by about 100 km. Both the AxAC and the AyAC may be identified best on February 12 by means of two large warm SST patches at the respective locations. As the positions of the previously (cf. Figure 6) diagnosed cyclonic eddies are identical with the northward directed cold intrusions, it is likely that the "eddies" are in reality cyclonic AMC meanders.

3.3 Vertical sections and profiles

In Figures 22 – 25, zonal and meridional vertical sections of geostrophic flow, potential density, temperature, and salinity are presented. Only the top 400 dbar are shown because the gradients of all quantities tend to become rather weak below as seen before. For the sound velocity sections in Figures 27, the vertical scale was extended to 700 dbar in order to visualize the main sound channel depth. All zonal sections are positioned at 36°00′N, and the longitude of the meridional sections is 31°10′E. The intersection point of the sections is indicated by the cross in most of the previously shown maps.

3.3.1 Geostrophic flow

All sections shown in Figure 22 reveal a surface intensified geostrophic flow. Near the sea surface, the maximum velocities reach up to 40 cm s^{-1} , and due to strong vertical shear velocities are generally less than 5 cm s^{-1} below about 350 dbar. At 36°N, the dominating signals are two high velocity bands centred at about 30°40′E and 31°40′E, which are due to the azimuthal jet of the AyAC (cf. Figures 6 and 7). When looking downstream, it can be seen that the jet is asymmetric, the high velocity core is always shifted to the left. This is due to the dynamical constraint that on the rotating earth the growth of cyclonic relative vorticity (i. e. the positive horizontal shear of the flow) is unlimited, whereas the growth of anticyclonic relative vorticity (negative shear) cannot exceed the absolute value of the Coriolis parameter. Another band of high northward velocity at the left end of the section is part of the AxAC jet. The asymmetry of the AyAC jet is also visible from the 31°10′E section on leg 1/2, but not from the corresponding one on leg 1/1, because of the previously mentioned missing CTD station no. 3 at 36°N.

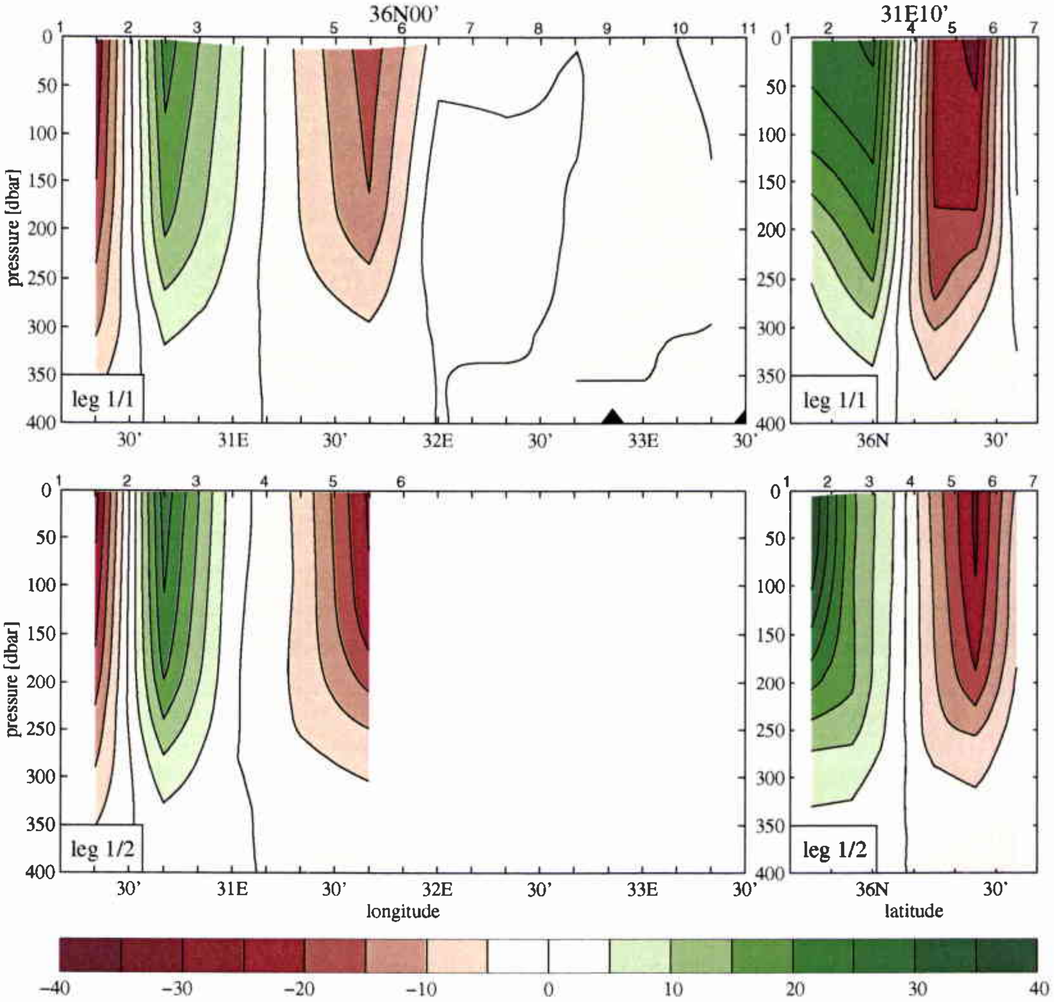

Figure 22 *Zonal (left) and meridional (right) sections of geostrophic flow [cm s^{-1}] relative to 900 dbar along 36°00′N and 31°10′E for leg 1/1 (top) and leg 1/2 (bottom). Green colours denote positive flow direction to the north and east, red colours negative flow direction to the south and west. Numbers on top of each section refer to the position of CTD stations.*

3.3.2 Temperature, salinity and potential density

Zonal and meridional sections of temperature, salinity and potential density are shown in Figures 23 – 25 Note that on leg 1/1 the CTD cast at (31°10′E, 36°N) is missing due to the malfunction of the temperature sensor mentioned above. Hence, care should be taken when interpreting any horizontal gradients of all quantities between casts no. 3 and 5 in the zonal section and between no. 2 and 4 in the meridional one, because these are created by horizontal interpolation of the contouring routine and must not be interpreted in terms of physical processes.

On leg 1/1, the figures clearly reveal that the core of the AyAC (about casts 3–5 in all sections) contains a pool of warm, saline, and light water. The temperature distribution in the centre of the AyAC represented by CTD cast no. 4 in the 31°10′E section is nearly homogeneous between the sea surface and about 300 dbar, the vertical temperature decrease is slightly more than 0.2°C. By contrast, in regions of cyclonic flow represented by casts no. 1 and 6 of the meridional section and by casts no. 2 and 6 of the zonal section, the same decrease of temperature occurs within the top 20 and about 100 dbars, respectively. There, the difference between the surface and about 300 dbar is about ten times larger of the order of 3°C. Qualitatively, the salinity distribution is similar; high and low salinity are correlated with high and low temperature, respectively. The ratio of the vertical salinity differences between the centres of anticyclonic and cyclonic eddies is of the same order of magnitude as temperature. In the anticyclones, the salinity difference between the surface and 300 dbar is more than 0.02 psu and in cyclones about 0.3 psu.

The major difference between the temperature and salinity structures is that temperature decreases monotonically with depth nearly everywhere, whereas the salinity field exhibits interleaving patterns mainly in the southern half of the meridional section between casts 1 and 4 and in the vicinity of cast no. 5 of the zonal section. The vertical scale of the interleaving is of the order of 10 m and the horizontal scale of the order of 10 km. In the same region, both temperature and salinity exhibit well defined vertical step structures, indicators of double-diffusive mixing.

As both temperature and salinity generally increase with depth, they have an opposite effect on the vertical rate of change of density. The vertically decreasing temperature leads to a density increase and stabilizes the stratification, whereas the vertical decrease of salinity reduces the density and causes destabilization. Quantitatively, a decrease of temperature of 0.2°C has about the same effect as increasing the salinity by 0.07 psu; both lead to an increase of density by 0.05 kg m^{-3}, which is the contour interval selected in Figure 25. Hence, at cast no. 4 in the meridional section, overturning down to about 300 m depth can be achieved if the surface temperature drops by only 0.2°C without changing the salinity, or by increasing the surface salinity by solely 0.07 psu. In contrast, at casts no. 1 and 6, such temperature and salinity changes would induce vertical mixing to about 50 and

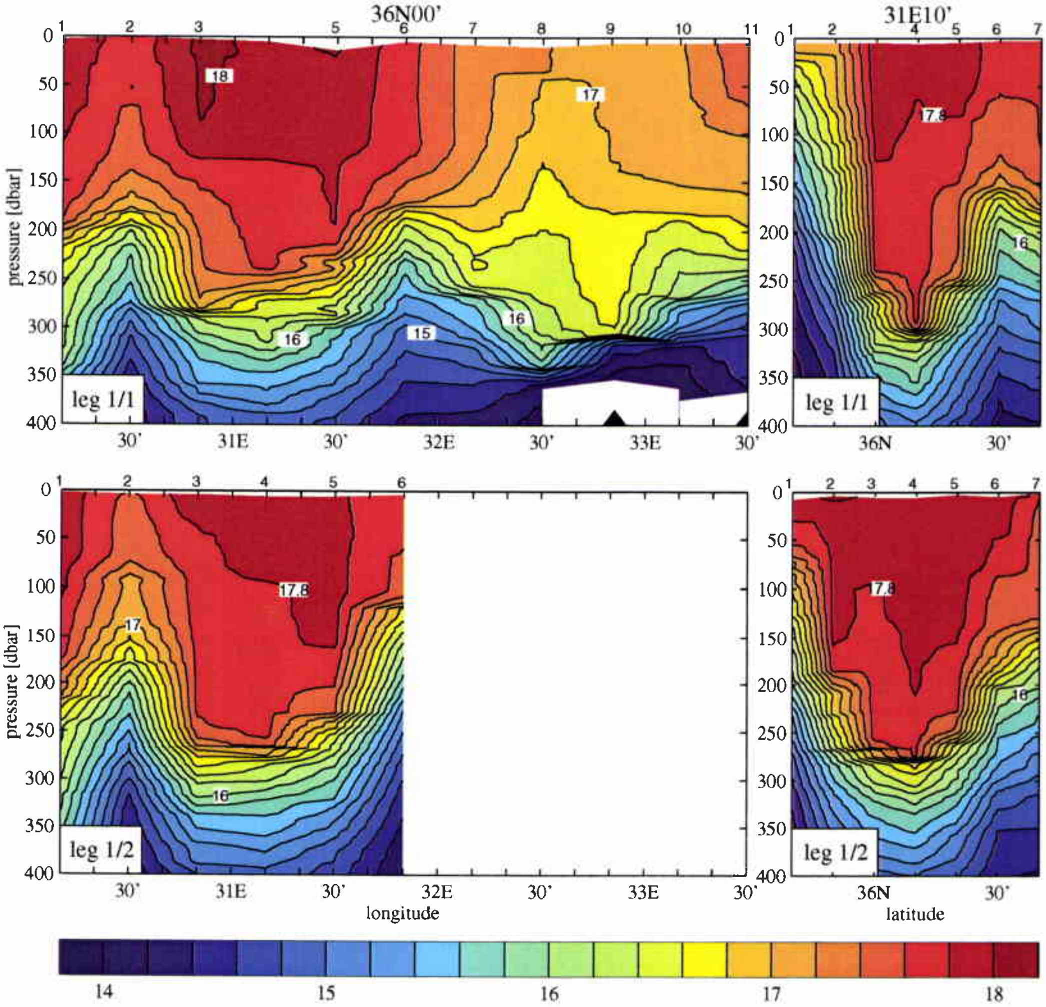

Figure 23 *Zonal (left) and meridional (right) sections of temperature [°C] along 36° 00′ N and 31° 10′ E for leg 1/1 (top) and leg 1/2 (bottom). Numbers on top of each section refer to the position of CTD casts.*

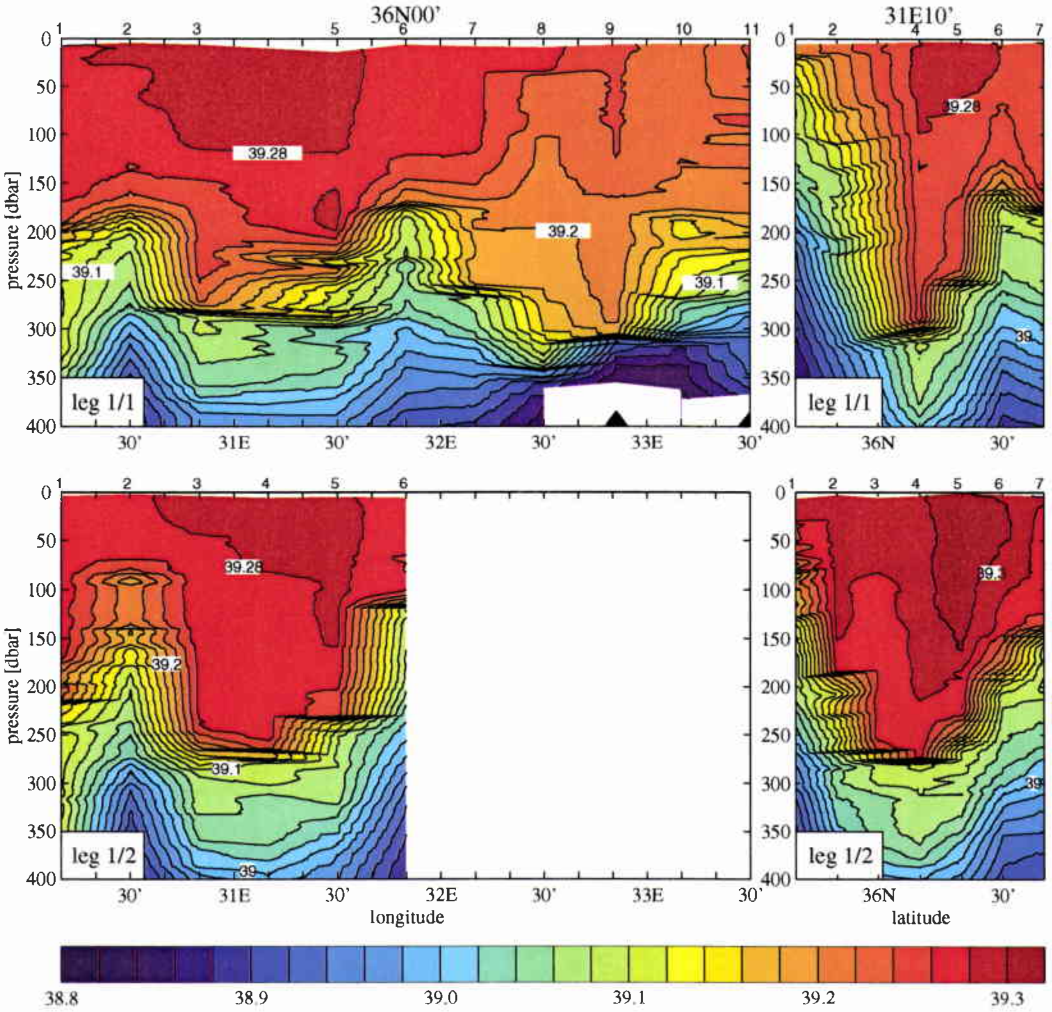

Figure 24 *Same as Figure 23, but for salinity [psu].*

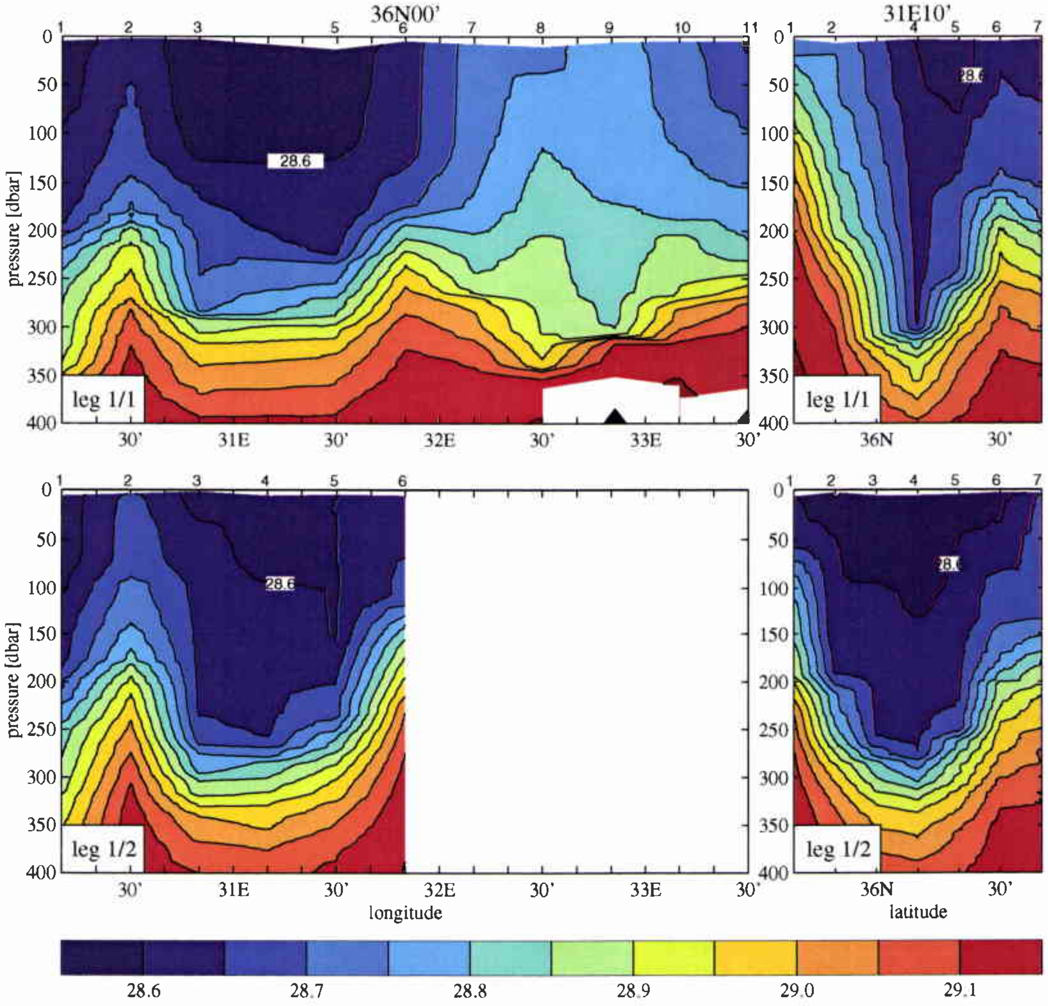

Figure 25 *Same as Figure 23, but for potential density* σ_0 *[kg* m^{-3} *].*

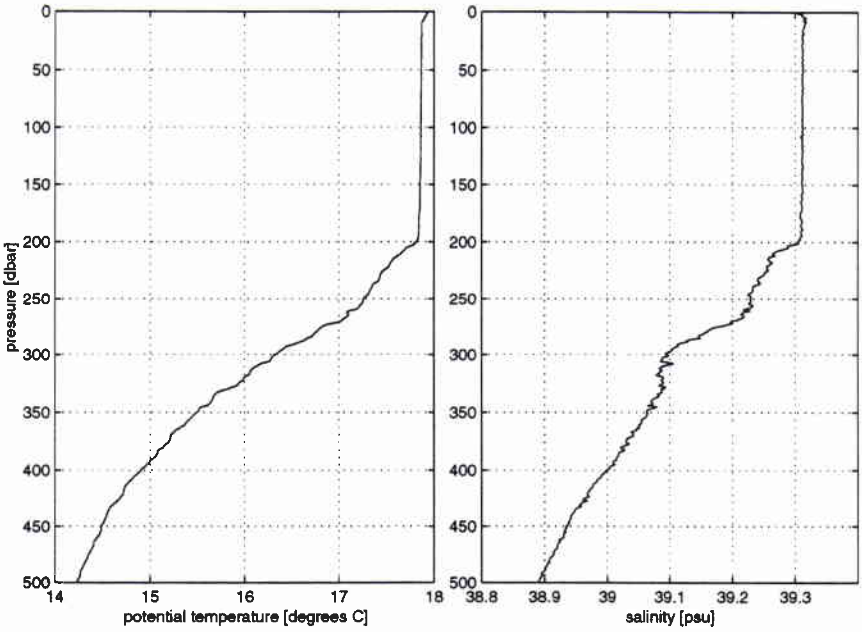

Figure 26 *CTD profiles of potential temperature and salinity measured during leg 2 on February 18 at (31°20.75′E, 36°8.30′N).*

100 m, respectively. In the 36°N section, preferred location for such thermohaline convection to more than 200 m would be in the AxAC (cast no. 1), in the AyAC (cast no. 5), and in the vicinity of cast no. 9. At the location of the other casts, convection to only 150 m or less would be possible. Hence, in the upper 300 metres, the stratification in the centres of anticyclonic eddies is potentially unstable with respect to slight surface loss of heat and freshwater, whereas the same is true for about half the vertical extent or less in regions of cyclonic flow.

The general situation on leg 1/2 does not differ fundamentally from that of leg 1/1, but there are some changes which have to be addressed. In the 31°10′E section of leg 1/1, there is clear evidence that the interior of the anticyclone is warmer and saltier on leg 1/2 expressed by the wider extent of the 17.8°C isotherm and the 39.28 psu isohaline. Comparison with Figures 15 – 18 suggests this to be perhaps an effect of the translation and change of shape of the AyAC. However, this explanation does not obtain for the appearence of the high salinity patch between casts no. 4 and 6 down to 162 m depth. Here, the salinity exceeds 39.3 psu, whereas on leg 1/1 the salinity was lower everywhere within this section. As mentioned above, on leg 1/1 salinities higher than 39.3 psu were encountered only at one station in the depth range between the surface and about 50 m depth, whereas on leg 1/2 such high salinites were diagnosed at 5 stations. As all these stations were sampled by *Çubuklu* with the same CTD probe, it can be excluded that this is an artefact of the *Çubuklu* salinity correction. Therefore, one must conjecture that the surface density has increaseed by an amount, which is sufficient to induce vertical overturning of the water column down to 162 m depth north of the centre of the AyAC. At the same time, the surface salinity must have increased by evaporation.

The profiles shown in Figure 26 reveal that after leg 1/2 convective processes even to greater depths must have taken place in this region. These profiles have been measured on leg 2 at a location corresponding approximately to the centre of the AyAC. Except for the very upper 8 dbar both temperature and salinity are homogeneous within the top 195 dbars. The rms potential temperature over this depth range is 8.5 mK and the rms salinity 0.0011 psu. Thus, it is extremely likely that intense vertical mixing has occurred in the recent past, because such a degree of vertical homogeneity was not observed on legs 1/1 and 1/2.

3.3.3 Sound velocity

Sections of sound velocity displayed in 27 reveal a completely different sound velocity structure in regions of anticyclonic and cyclonic flow. In the first, there is a minimum at the sea surface, the velocity then increases to maximal values between about 200 and 300 dbar depth and decreases again below until it reaches an absolute minimum between 400 and 500 dbar, which is the depth of the main sound channel axis. This typical situation is found in the zonal sections between CTD casts no. 3 and 5 and in the central region of the meridional sections occupied by the AyAC. The maximum at intermediate depth is completely missing in regions of strong cyclonic flow, for example at cast no. 1 in the meridional sections. Here, the sound velocity is maximal at the sea surface and then decreases continuously downward until it reaches the sound channel axis located between 200 and 400 m dbar. At all other locations which are not characterized by pronounced anticyclonic or cyclonic flow, the situation is mixed. For example, at casts no. 2, 8, and 9 in the zonal sections, a relative mimimum of sound velocity is found at the sea surface, a weak intermediate maximum exists between about 150 and 300 dbar and the sound channel minimum is at about 400 dbar depth.

As the salinity variations in the survey area are generally too small to have a significant effect, the diagnosed variations of the sound velocity can be fully explained in terms of temperature and pressure. In regions of anticyclonic flow, it was found before that the temperature is homogeneous in the upper about 300 dbar. Hence, vertical changes of sound velocity are fully controlled by pressure in this depth range creating the minimum at the sea surface and the intermediate maximum between 200 and 300 dbar. Below, the rapidly decreasing temperature overcompensates for the effect of pressure increase leading to a decrease of sound velocity until the depth of the sound channel axis is reached, where the sound velocity again increases due to the increasing pressure and weak temperature gradients. In regions of cyclonic flow, there is no thick isothermal upper layer and the intermediate maximum is missing

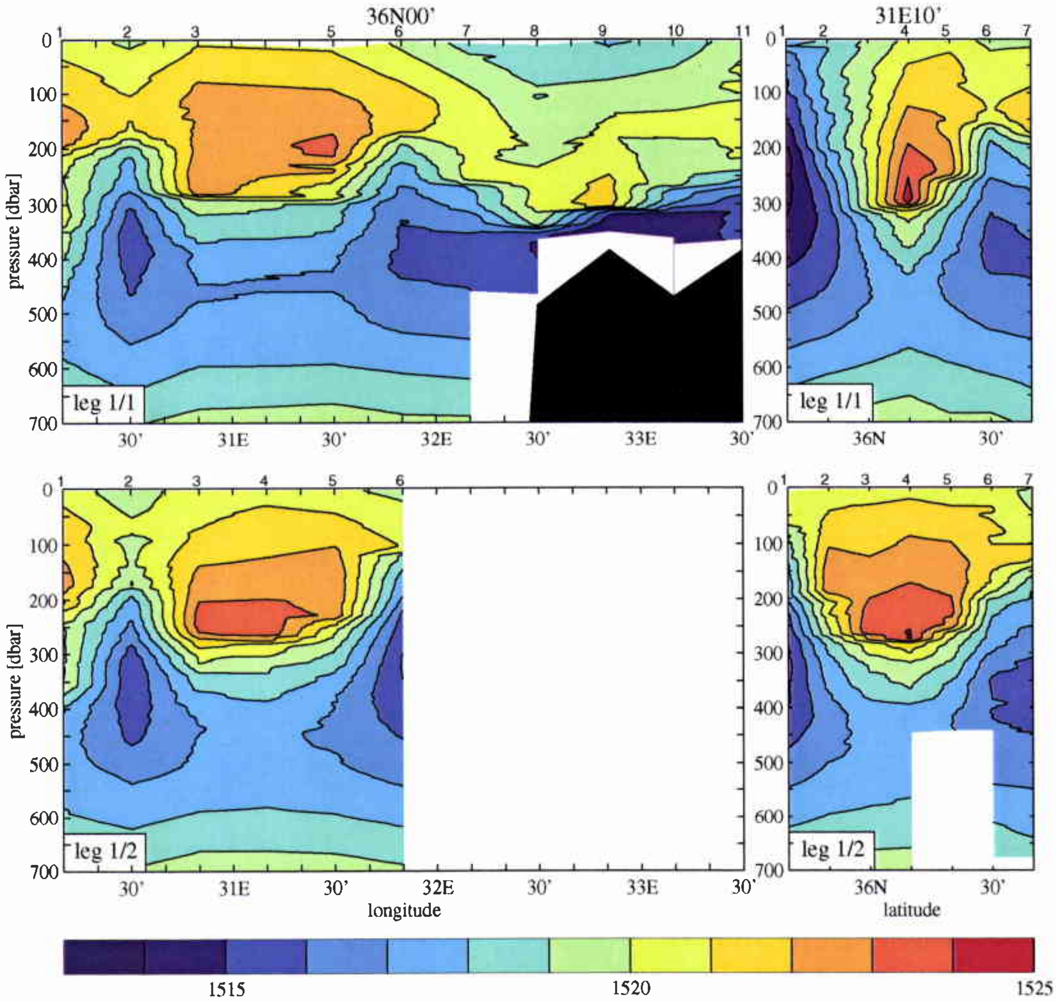

Figure 27 *Same as Figure 23, but for sound velocity [m s^{-1}].*

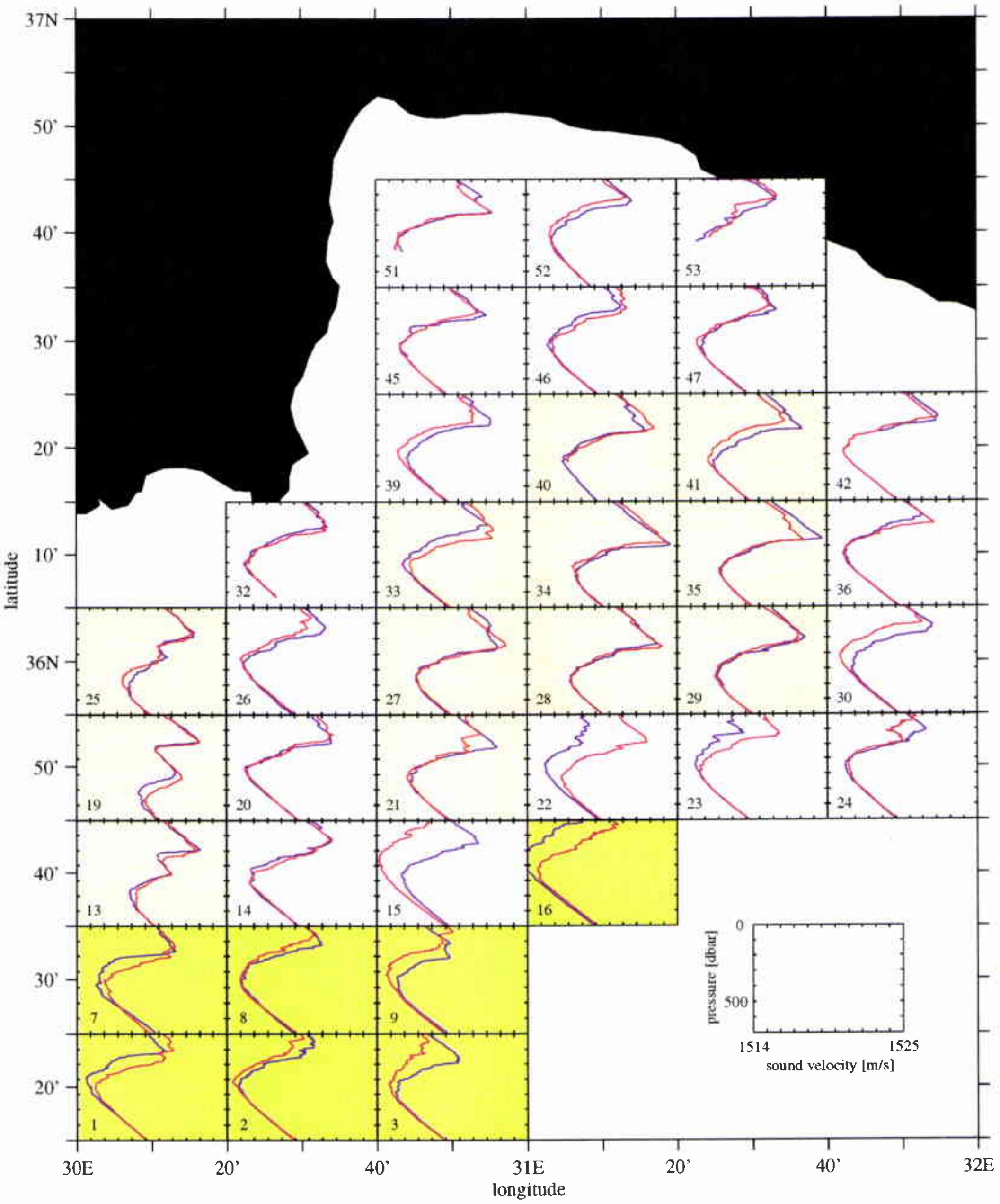

Figure 28 *Regional distribution of sound velocity profiles on leg 1/1 (blue) and leg 1/2 (red). The profiles correspond to CTD stations located at the centre position of each subplot. The axes scaling is defined in the inset in the bottom right corner. For the different colors of the axes back planes see text.*

Table 1 *Water mass definitions in the Levantine Basin according to [13].*

water mass	temperature range [°C]	salinity range [psu]
LSW	≥16.5	≥39.05
AW	15.8–17.0	38.60–38.80
LIW	15.0–15.8	38.95–39.11
LDW	≤14.1	≤38.87

because of strong temperature stratification.

Large scale differences and temporal variations of the sound velocity structure can be deduced from Figure 28. Sound velocity was calculated only from those CTD casts which were occupied both during legs 1/1 and 1/2 and plotted at the corresponding horizontal positions. The subplots of those locations where the minimum sound velocity of the main sound channel axis is higher than 1515 m s^{-1} or the maximum sound velocity exceeds 1523 m s^{-1} in the 200–300 dbar depth range, are marked by yellow axes back panels. Here, the depth of the main sound channel axis lies generally at 400-500 dbar depth. These profiles clearly correspond to the approximate locations of the AxAC and AyAC, hence both anticyclones are areas of high sound speed and a deep sound channel according to their deep reaching warm cores. In contrast, green axes back panels denote profiles, where the sound velocity maximum is generally less than 1521 m s^{-1} and the absolute minimum is always less than 1515 m s^{-1} . The sound channel depth is shallow at about 300 dbar. In many cases, either on leg 1/1 or leg 1/2, these profiles do not exhibit a well pronounced intermediate maximum, because these regions are occupied by strong cold cyclones. All other profiles (white axes back panels) correspond to regions of weaker cyclonic or anticyclonic flow and do not exhibit either of the extremes. A peculiarity worth to be mentioned can be seen in subplots 13, 19, and 25. Here, at the location of the AxAC, a secondary sound velocity maximum lies at 300-400 dbar. This is caused by a thermostad found at 200–600 dbar below the main thermocline.

The strongest temporal changes are found in subplots 3, 9, 15, 16, 22, 23, 24, and 30, i. e. they are confined to the southeastern boundary of the survey area. The sound velocity structure is significantly different from one leg to the other, which is caused by displacement of the AMC front due to travelling meanders.

3.4 *Water masses*

According to [14], the major water masses existing in the survey area are the Levantine Surface Water (LSW), AW, LIW, and Deep Water (DW). In this study, the

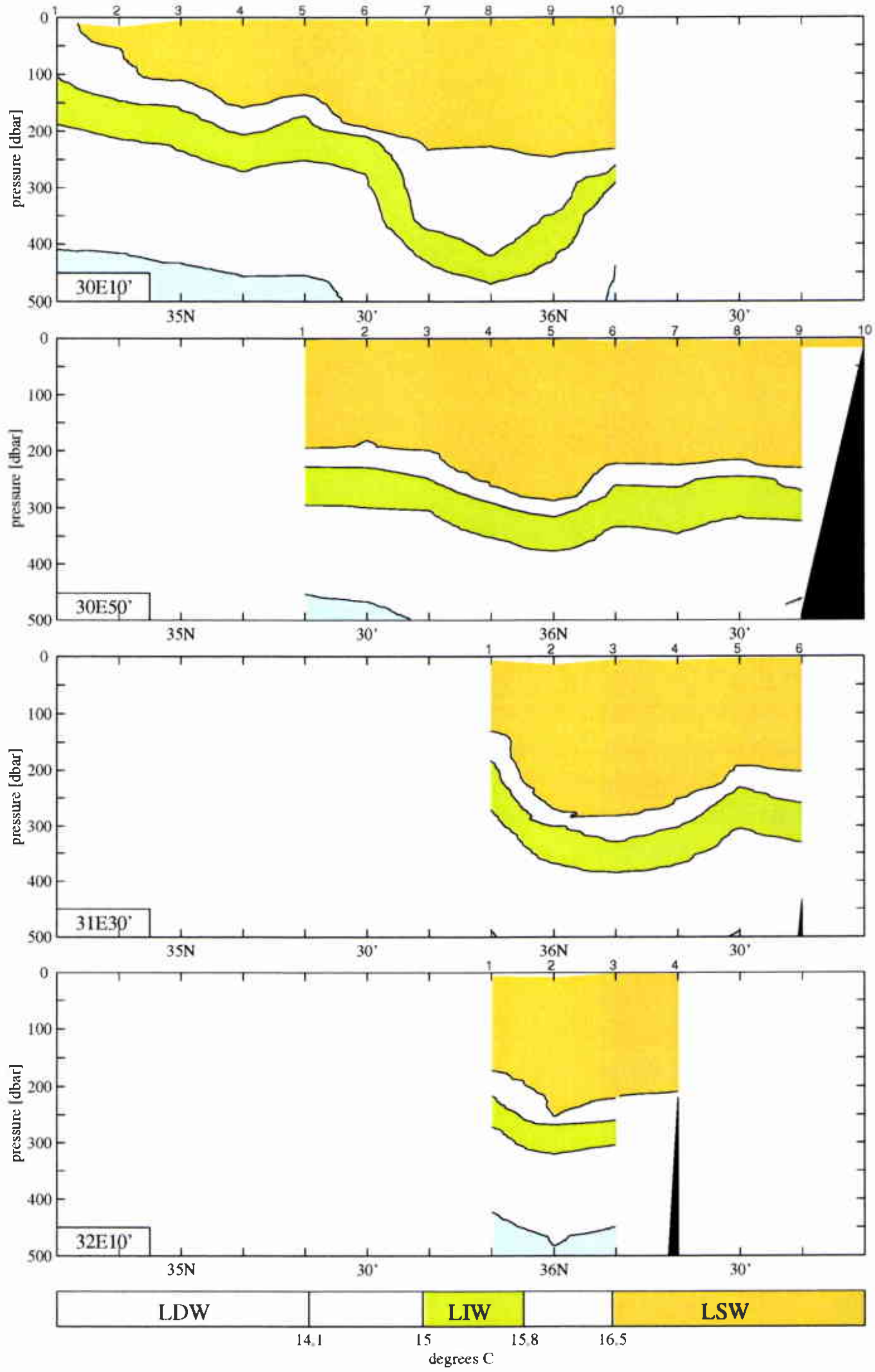

Figure 29 *Meridional water mass distribution of the top 500 dbar on leg 1/1 at 30° 10′ E, 30° 50′ E, 31° 30′ E, and 32° 10′ E. The water mass ranges of LDW, LIW, and LSW are indicated by different colours according to Table 1. The selected colour code corresponds to that in Figure 4. Small numbers on top of the sections refer to the position of CTD casts.*

revised definition published recently by [13] will be used, because the temperature and salinity ranges of all water masses are precisely defined as shown in Table 1. As [13] distinguished between different types of DW, LDW (Levantine Deep Water) will be used instead of DW.

The water mass ranges as defined in Table 1 are shown in Figure 4. As that figure contains all CTD data, the first result is that AW was not present in our survey area. This is consistent with [4], who did not find any AW in this region in winter. AW is characterized by a near surface salinity minimum, which vanishes in winter as a result of vertical convective processes ([15]). However, traces of AW were identified during leg 1/1 at (35°50′N, 30°30′E), about 35 km southeast of the centre of the AyAC, where a salinity minimum of 39.004 psu was found at 148 dbar depth, clearly visible at a temperature of about 15.9°C above the LIW box in Figure 4.

All other water masses are present in selected meridional sections shown in Figure 29. LSW, defined by temperatures above 16.5°C, is found nearly everywhere in the survey area. In regions of anticyclonic flow LSW attains a vertical extent of more than 250 dbar, in regions of cyclonic flow, the LSW containing layer is shallower. An absolute minimum occurs at CTD cast no. 1 in the 30°10′E section, where the layer thickness drops to zero. The thickness of the LIW layer is between 50 and 100 dbar everywhere. It reaches maximum depths of more than 350 dbar in the centre of the AyAC and even more than 450 dbar in the AxAC. Towards the AMC front and in regions of cyclonic flow it lies closer to the surface. A minimum depths of 100 dbar is found at cast no. 1 in the westernmost section. The upper bound of the deepest water mass, LDW, is correlated in the same way with the flow field. Maximum depth values of its upper bound of more than 500 dbar are attained in the centre of the AyAC, whereas minimum values around 450 dbar are found in the cyclone centres and close to the coast.

4

Discussion and conclusions

4.1 *Horizontal circulation patterns*

The key features of the near suface horizontal flow field in our survey area are the CC, the AMC, the AyAC, and the AxAC. Each of these features has been documented in the past, but in many cases, when one was observed, another one was absent. In order to find out which of these features are permanent or recurrent and what relationship might exist between them, Table 2 was constructed to emulate that of [1], summarizing all observations by [1], [4], [15], and the present survey.

There is strong evidence for a relationship between the existence of the AyAC and the AMC, i.e. columns 1 and 2 of Table 2, in which the present survey is labelled "+S". The AyAC is present, the AMC does not flow immediately offshore but is confined to a path about 100 km south. The same situation is found in surveys 1, 2, 5, and 8. Except for survey 3 ("+SN") all other survey patterns can be described by "–N". Hence, a southern flow path of the AMC is probably a necessary and sufficient condition for the existence of the AyAC. A similar relationship appears to exist between the CC and the AxAC. They are present in all surveys ("++" in columns 3 and 4), except for surveys 2 and 5, where both are absent ("– –") giving rise to speculation, as to why a "– –" in columns 3 and 4 occurs only when "+S" occurs in columns 1 and 2. Thus, there is weak evidence that the AyAC in conjuction with a southern flow path of the AMC are necessary conditions for the disappearance of CC and AxAC. In other words, the non-existence of AyAC and a near-shore flow path of the AMC are always accompanied by CC and AxAC.

If survey 4 is ignored, one can identify four different flow patterns in Figure 30 denoted by roman numbers I to IV. These patterns reveal that the AMC is the northern part of the West Cyprus Cyclone (I–IV), which is occasionally fed by the CC (I–III). In pattern I, the West Cyprus Cyclone extends north into the Antalya Basin, there is no AyAC, and CC joins the northwestward cyclonic flow along the coast immediately west of Cyprus. Patterns III and IV are dominated by the AyAC blocking a near-shore northwestward current and forcing the AMC to a flow path south of the AyAC. In III, the CC joins the AMC again, in IV, however, the connection between the AMC and the CC is interrupted, and the CC reverses direction. A characteristic feature of this pattern is that the AyAC covers the entire Antalya Basin extending far to the south. It may be divided into several centres and the

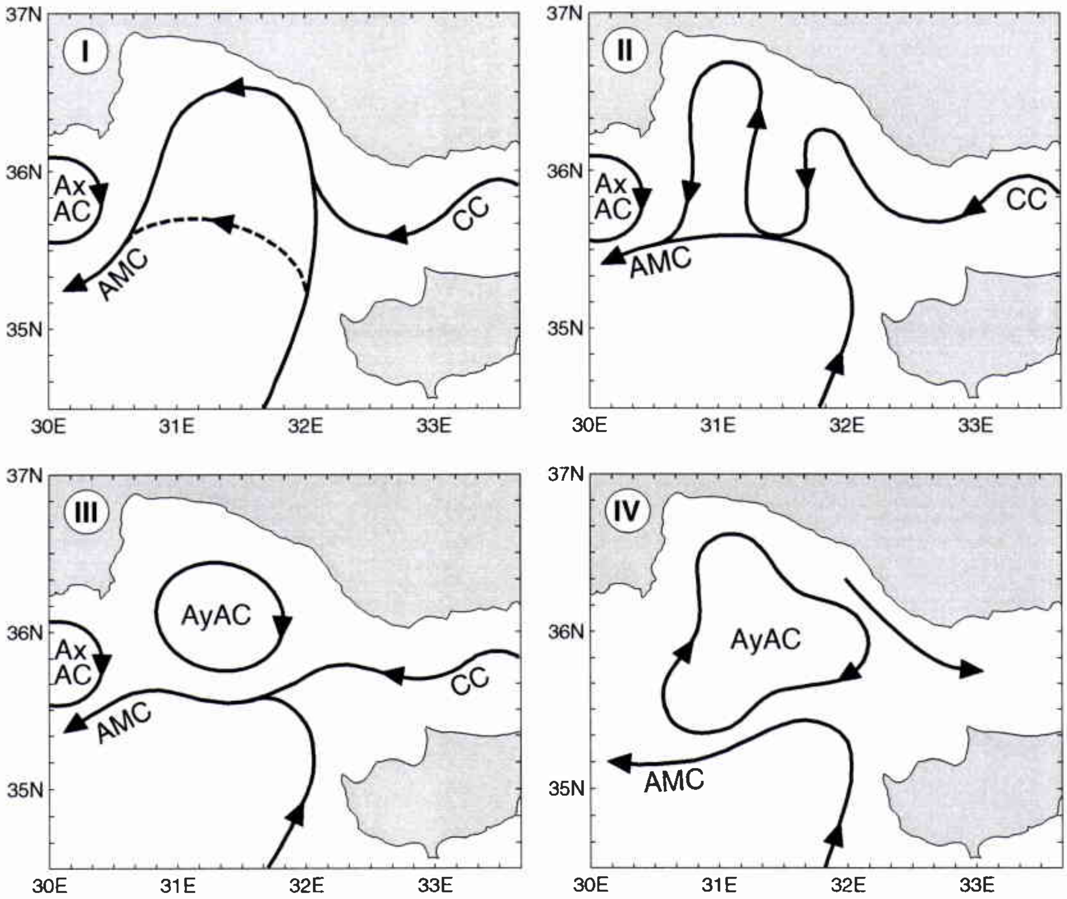

Figure 30 *Near surface circulation patterns of the Antalya Basin based on a literature search. Pattern III resembles best the situation of the present survey.*

Table 2 *Upper ocean features of the Antalya Basin. –=not present, +=present, N=flow path along the coast, S=flow path distant from coast, ?=not enough information. The roman numbers in the last column refer to the respective situation depicted in Figure 30.*

survey no.		Antalya Anticyclone	Asia Minor Current	Cilician Current	Anaximander Anticyclone	
1	Nov-Dec 85	+	S	+	+	III
2	Mar-Apr 86	+	S	–	–	IV
3	Jun 86	+	SN	+	+	II
4	Mar-Apr 87	–	N	+	?	(I)
5	Jun 87	+	S	–	–	IV
6	Aug-Sep 87	–	N	+	+	I
7	Jul 88	–	N	+	+	I
8	Oct 88	+	S	+	+	III
9	Mar 89	–	N	+	+	I
10	Aug 90	–	N	+	+	I
11	Feb 97	+	S	+	+	III

AxAC has disappeared. It may have been entrained into the AyAC. A special situation is depicted by II. The AMC is again composed of the northern rim flow of the West Cyprus Cyclone and the CC, but it is difficult to identify the path of AMC because the entire Antalya Basin is occupied by cyclonic and anticyclonic eddies. Therefore, the notation "SN" was introduced for the second column of the June 1986 survey in Table 2.

The sequence of the sketches I–IV was arranged to provide tentative insight into the life cycle of the Antalya Basin horizontal circulation. Pattern I, defined as the starting point of the cycle, is characterized by a strong near-shore AMC. The AMC starts meandering due to hydrodynamic instability ([15], [16]) and fills the basin with a few (1–3) cyclones and anticyclones (II). In a special situation, a large anticyclone may be pinched off from the coastal current to form the AyAC (III). The near-shore flow path of the CC is blocked and if the AyAC is powerful enough, it may even reverse direction (IV). The way, in which the life cycle is closed to reassume pattern I, is open to speculation. Due to dissipation, the AyAC surely will weaken and may finally disappear. Another possibility would be that the AMC at the southern rim of the AyAC becomes unstable and that at least parts of the AyAC escape to the south by evolving anticyclonic meanders. This is perhaps the mechanism, by which warm and salty anticyclones find their way from the Asia Minor coast into the central Levantine Sea as postulated by [17] and [18].

4.2 Spatial and temporal variability

The horizontal scales of mesoscale variability are expected to be of the order of 2π times the internal Rossby radius. According to [2], the Rossby radius in the Northern Levantine Sea is about 10–15 km, hence the horizontal resolution of the survey (1/6° in latitude and 2/6° in longitude) was sufficient to resolve the mesoscale structures. The nominal horizontal spacing of the majority of the POEM surveys was 1/2° intended for resolving basin and sub-basin scale features as depicted in Figure 30(III). In reality, the sub-basin scale patterns are superimposed by mesoscale structures. It was found that both the CC and the AMC exhibit meanders with wavelengths of nearly 100 km, which suggests that they are baroclinically unstable. The diameters of fully detached individual eddies are expected to be only half of that. The only individual eddies which were covered completely by our survey, were the AyAC and two cyclones trapped between the AyAC and the Turkish coast, all exhibiting a diameter between about 40 and 60 km.

As the major portion of the Antalya Basin was surveyed twice within about a week, it was possible to investigate temporal changes. From the displacement of crests and troughs the phase speed of meanders of the AMC and the CC was estimated at 10 cm s^{-1} . Although from the displacement alone and from AVHRR images it was not possible to decide, whether they travel to the west or to the east, westward propagation is plausible, because according to theory ([19]) the phase speed of unstable meanders is expected to be about half of the mean current speed. In our case, the near surface current is of the order of 50 cm s^{-1} , hence a mean speed of 10 cm s^{-1} over the upper 1000 dbar depth range is resonable. It was also possible to show that the AyAC was not stable with respect to its position and shape. The centre position was different by about 10–20 km in both surveys, but the centre seems to oscillate around a mean position suggesting that the AyAC is confined to the Antalya Basin and not displaced immediately by the AMC. There is, however, clear evidence that the AyAC interacts strongly with the AMC. Figures 16 and 10 show that it draws in parts of the AMC at its southwestern side and advects them between the AyAC and the Turkish coast. Hence, the AyAC acts as a mixing agent, reducing the contrasts across the AMC front, which may lead to its own disappearance.

4.3 Water mass formation

From Figure 24 it was conjectured that at the northern periphery of the AyAC, air-sea interaction had increased the surface density by an amount which enabled convection from the surface to about 160 m depth within the period of time between legs 1/1 and 1/2. From Figure 26 it was further deduced that the convection persisted for a further number of days, creating an homogeneous mixed-layer of up to about 200 m thickness in the centre of the AyAC. It can be excluded that this mixed-layer deepening was solely due to wind mixing, because the wind speed was always less than 6 m s^{-1} between February 9 and 18 (it was also low during the port calls of the ships from February 14–16), and wind mixing alone would not have increased the mixed-layer salinity. Hence, the convection can only be driven by buoyancy loss due to evaporation and/or net surface cooling.

According to Figures 23, 24, and 25 for thermally-driven convection to extend to about 200 m depth it would be necessary for the water column to cool by an order of ΔT =–0.1°C. The following calculation will show that this is possible within 10 days. The necessary heat loss rate would be

$$H = \frac{m\ c_p\ \Delta T}{\tau} \approx -80\ \mathrm{Wm}^{-2},$$

where $m \approx 2 \cdot 10^5$ kg is the mass of the water column assuming a base of 1 m^2, $c_p \approx 4 \cdot 10^3$ J kg^{-1} K^{-1} the specific heat, and $\tau \approx 10^6$ s representing a period of 10 days. This number is comparable to the February value for the climatological total surface heat loss in this region [5] amounting to about –100 Wm^{-2}. Similar values are obtained by making an estimate based on the meteorological observations. Here, the heat loss due to the flux of latent and sensible heat is ≈ -100 Wm^{-2} (Figure 5). Assuming an additional longwave radiation heat loss of ≈ -40 Wm^{-2} and a shortwave radiation gain of $\approx$100 Wm^{-2} (typical values for this latitude and time of the year ([20])), we obtain a net heat loss of ≈ -60 Wm^{-2}. Taking into account that additional buoyance loss is caused by the simultaneous increase of surface salinity, it is extremely likely that the observed homogenization in the centre of the AyAC is due to thermohaline surface forcing.

The following estimate will show that evaporation is able to increase the salinity of the same water column by the order of 0.01 psu over the same period of time. The salinity s (now in ppt) is defined as

$$s = 1000\frac{m_s}{m},$$

where m_s is the salt mass and $m = m_s + m_w$ the mass of seawater with m_w being the mass of pure water. Finite changes Δm_w and Δs are related by

$$\Delta m_w = -m\frac{\Delta s}{s},$$

hence $\Delta m_w = -50$ kg using $m \approx 2 \cdot 10^5$kg, $\Delta s = 10^{-2}$ ppt, and $s \approx 40$ ppt, which is approximately equivalent to –50 mm in sea level height. According to [5], the monthly climatological freshwater flux in the eastern Mediterranean in February is about –100 mm $month^{-1}$ or –33 mm within 10 days, which is at least of the same order of magnitude. The freshwater flux evaluated directly from the meteorological measurements (Figure 5) yields a mean evaporation rate of about –3 mm day^{-1}amounting also to the same number of about –30 mm within 10 days.

The above calculations show that in the eastern Mediterranean, water mass formation may take place in two locations — cyclones *and* anticyclones. Both induce convection by different types of preconditioning: As doming or outcropping of isopycnals in cyclones induces low vertical stability, surface buoyancy loss leads rapidly to convective overturning, which may extend to great depths in case of large losses. In anticyclones, because of the bowl-shape of isopycnals, the thermocline lies at greater depths and the water pool above is weakly stratified. In this case, surface buoyancy loss leads to further homogenization of the pool and may also deepen the mixed-layer, however, mixing to greater depths is prevented by the thermocline. As both in the cyclonic and the anticyclonic case convection is able to homogenize the water column to a few hundred metres depth, both are likely formation regions for LIW. Although in the present survey the homogeneous pool of water in the AyAC was too warm and salty to be classified as LIW, it may contribute to LIW by vertical mixing with the underlying water body. This will lower its temperature and also its salinity towards the LIW temperature/salinity relationship as defined in Table 1. As warm and salty water lies above colder and fresher water, double diffusion is a possible vertical mixing mechanism. Estimating the density ratio

$$R = \frac{\alpha T_z}{\beta S_z}$$

from Figures 23 and 24, where α, β are the thermal and haline expansion coefficients, and T_z, S_z the vertical gradients of temperature and salinity respectively, yields values in the range between 2 and 2.5, hence super-critical growth of salt fingers is extremely likely ([21]). In addition, as the anticyclonic eddies are known to be enduring features (order of years), the timescale is sufficient for the trapped water body to undergo a significant transformation before it is released as LIW into the permanent thermocline.

5

Glossary

ADCP = Acoustic Doppler Current Profiler
AMC = Asia Minor Current
AVHRR = Advanced Very High Resolution Radiometer
AW = Atlantic Water
AyAC = Antalya Anticyclone
AxAC = Anaximander Anticyclone
CC = Cilician Current
CTD = Conductivity-Temperature-Depth (probe)
DGPS = Differential Global Positioning System
DW = Deep Water
LDW = Levantine Deep Water
LIW = Levantine Intermediate Water
LSW = Levantine Surface Water
MMJ = Mid-Mediterranean Jet
POEM = Physical Oceanography of the eastern Mediterranean
SST = Sea surface temperature
UTC = Universal Time Coordinate
XBT = Expendable Bathythermograph

6

Acknowledgements

This work was performed at the SACLANT Undersea Research Centre in La Spezia (Italy). The support of the Turkish Navy Department of Navigation, Hydrography and Oceanography (Istanbul) and the skill and willingness of the crews of NRV *Alliance* and TCG *Çubuklu* are greatly acknowledged. The AVHRR images were provided by E. Nacini. I would like to thank also A. Legner for his help with the drawings.

References

[1] A. R. Robinson, M. Golnaraghi, W. G. Leslie, A. Artegiani, A. Hecht, E. Lazzoni, A. Michelato, E. Sansone, A. Theocharis, and Ü. Ünlüata. The Eastern Mediterranean general circulation: features, structure and variability. *Dyn. Atm. Oceans*, 15:215–240, 1991.

[2] E. Özsoy, A. Hecht, and Ü. Ünlüata. Circulation and hydrography of the Levantine Basin. Results of POEM coordinated experiments 1985–1986. *Progr. Oceanogr.*, 22:125–170, 1989.

[3] POEM Group. General circulation of the Eastern Mediterranean. *Earth Science Reviews*, 32:285–309, 1992.

[4] E. Özsoy, A. Hecht, Ü. Ünlüata, S. Brenner, T. Oğuz, J. Bishop, M. A. Latif, and Z. Rozentraub. A review of the Levantine Basin circulation and its variability during 1985–1988. *Dyn. Atm. Oceans*, 15:421–456, 1991.

[5] M. Zavatarelli and G. L. Mellor. A numerical study of the Mediterranean Sea circulation. *J. Phys. Oceanogr.*, 25(6):1384–1414, 1995.

[6] G. Wüst. On the vertical circulation of the Mediterranean Sea. *J. Geophys. Res.*, 66(10):3261–3271, 1961.

[7] I. M. Ovchinnikov. The formation of Intermediate Water in the Mediterranean. *Oceanology*, 24(2):168–173, 1984.

[8] S. A. Morcos. Sources of Mediterranean Intermediate Water in the Levantine Sea. In A. L. Gordon, editor, *Studies in Physical Oceanography*, volume 2, pages 185–206. Gordon and Breach, New York, 1973.

[9] E. Özturgut. The sources and spreading of Levantine Intermediate Water in the Eastern Mediterranean. SACLANTCEN Memorandum SM–92, SACLANT ASW Research Centre, La Spezia, Italy, 1976. 45 pp.

[10] D. Georgopoulos, A. Theocharis, and G. Zodiatis. Intermediate Water formation in the Cretan Sea (South Aegean Sea). *Oceanol. Acta*, 12(4):353–359, 1989.

[11] F. P. Bretherton, R. E. Davis, and C. B Fandry. A technique for objective analysis and design of oceanographic experiments applied to MODE-73. *Deep-Sea Res.*, 23(7):559–582, 1976.

[12] National Geographic Data Centre. ETOPO5—5-minute grided elevations/ bathymetry for the world. In *Global Relief CD-ROM*. National Geographic Data Centre, Boulder, Colorado, 1993.

[13] P. Lermusiaux. Error subspace data assimilation methods for ocean field estimation. Harvard Open Ocean Model Reports: Reports in Meteorology and Oceanography 55, Harvard University, Cambridge, MA, 1997. 402 pp.

[14] A. Hecht, N. Pinardi, and A. R. Robinson. Currents, water masses, eddies and jets in the Mediterranean Levantine Basin. *J. Phys. Oceanogr.*, 18(10):1320–1353, 1988.

[15] E. Özsoy and Ü. Ünlüata. Physical oceanography of the Eastern Mediterranean. In N. F. R. Della Croce, editor, *Symposium Mediterranean Seas 2000*, pages 207–253. Università di Genova, Italy, 1993.

[16] Y. Feliks and M. Ghil. Downwelling-front instability and eddy formation in the Eastern Mediterranean. *J.Phys. Oceanogr.*, 23(1):61–78, 1993.

[17] S. Brenner. Structure and evolution of warm core eddies in the Eastern Mediterranean Levantine Basin. *J. Geophys. Res.*, 94(C9):12593–12602, 1989.

[18] Y. Feliks and S. Itzikowitz. Movement and geographical distribution of anticyclonic eddies in the eastern Levantine Basin. *Deep-Sea Res.*, 34(9):1499–1508, 1987.

[19] J. Pedlosky. *Geophysical Fluid Dynamics.* Springer Verlag, New York, 1987. 710 pp.

[20] H.-J. Isemer and L. Hasse. *The Bunker Climate Atlas of the North Atlantic Ocean*, volume Vol. 2: Air-sea interactions. Springer Verlag, Berlin, 1987. 256 pp.

[21] R. W. Schmitt Jr. The growth rate of super-critical salt fingers. *Deep-Sea Res.*, 26A:23–40, 1979.

Report no. changed (Mar 2006): SR-299-UU

Document Data Sheet

NATO UNCLASSIFIED

Security Classification UNCLASSIFIED		*Project No.* 022-3
Document Serial No. SR-299	*Date of Issue* July 1998	*Total Pages* 62 pp.

Author(s)

Onken, R.

Title

Oceanographic conditions in the Antalya Basin in winter.

Abstract

From an oceanographic survey of the Antalya Basin in February 1997 the following horizontal circulation pattern was found: The Asia Minor Current (AMC) was detached from the Turkish coast flowing to me southwest between 30°E and 33°E. The Cilician Current was present and feeding the AMC. The AMC exhibited meander wavelengths of about 100 km and phase speed circa 10 cm s^{-1}. A train of cyclonic eddies was located at the southern flank of the AMC. The central part of the Antalya Basin was occupied by the Antalya Anticyclone extending at least over the upper 100 dbar depth range. A second anticyclone further west was identified as the Anaximander Anticyclone. From a comparison with previous surveys it is concluded that the circulation of the Antalya Basin is controlled by the position of the AMC. The circulation is cyclonic, if the AMC flow path is confined to the coast, and anticyclonic, if the path is distant from coast. In the latter case, the anticyclonic flow may force the Cilician Current to reverse its direction.

A nearly homogenous pool of Levantine Surface Water extending down from the sea surface to about 250 m depth was found trapped within the Antalya Anticyclone. It is shown that even under light wind conditions, thermohaline convection down to about 200 m depth takes place in this pool. It is suggested that the convectively mixed water body is subject to further transformation by double diffusive mixing with the underlying water and finally contributes to the formation of Levantine Intermediate Water.

Keywords

Eastern Mediterranean – Levantine Basin – Antalya Basin – Antalya Anticyclone – Anaximander Anticyclone – Asia Minor Current – Cilician Current – Levnatine Intermediate Water – circulation – convection – sound velocity – variability

Issuing Organization

North Atlantic Treaty Organization
SACLANT Undersea Research Centre
Viale San Bartolomeo 400, 19138 La Spezia,
Italy

[From N. America: SACLANTCEN
(New York) APO AE 09613]

Tel: +39 0187 527 361
Fax:+39 0187 524 600

E-mail: library@saclantc.nato.int

Initial Distribution for SR-299

Ministries of Defence

DND Canada	10
CHOD Denmark	8
MOD Germany	15
HNDGS Greece	12
MARISTAT Italy	9
MOD (Navy) Netherlands	12
NDRE Norway	10
MOD Portugal	5
MDN Spain	2
TDKK and DNHO Turkey	5
MOD UK	20
ONR USA	32

NATO Commands and Agencies

NAMILCOM	2
SACLANT	3
CINCEASTLANT/ COMNAVNORTHWEST	1
CINCIBERLANT	1
CINCWESTLANT	1
COMASWSTRIKFOR	1
COMSTRIKFLTANT	1
COMSUBACLANT	1
SACLANTREPEUR	1
SACEUR	2
CINCNORTHWEST	1
CINCSOUTH	1
COMEDCENT	1
COMMARAIRMED	1
COMNAVSOUTH	1
COMSTRIKFORSOUTH	1
COMSUBMED	1
NC3A	1
PAT	1

Scientific Committee of National Representatives

SCNR Belgium	1
SCNR Canada	1
SCNR Denmark	1
SCNR Germany	1
SCNR Greece	1
SCNR Italy	1
SCNR Netherlands	2
SCNR Norway	1
SCNR Portugal	1
SCNR Spain	1
SCNR Turkey	1
SCNR UK	1
SCNR USA	2
SECGEN Rep. SCNR	1
NAMILCOM Rep. SCNR	1

National Liaison Officers

NLO Canada	1
NLO Denmark	1
NLO Germany	1
NLO Italy	1
NLO Netherlands	1
NLO Spain	1
NLO UK	1
NLO USA	1

Sub-total	188
SACLANTCEN	30
Total	218